Front. Earth Sci. 2022, 16(2): 411–434
https://doi.org/10.1007/s11707-021-0954-1

RESEARCH ARTICLE

Estimates of strength and cracking behaviors of pre-flawed granite specimens treated by chemical corrosion under triaxial compression tests

Zhicong LI, Richeng LIU (✉), Shuchen LI, Hongwen JING, Xiaozhao LI, Liyuan YU

State Key Laboratory for Geomechanics and Deep Underground Engineering, China University of Mining and Technology, Xuzhou 221116, China

Abstract Four types of granite specimens were prepared and treated by chemical corrosion for 5 and 30 days, which were then used to carry out triaxial compression tests under different confining pressures σ_3. Type A is the intact sample with no preexisting flaws. Types B and C are the samples containing two relatively low-dip flaws and two relatively high-dip flaws, respectively. Type D is the sample including both relatively low-dip and relatively high-dip flaws. The influences of pH value of chemical solutions, flaw distribution, corrosion time and σ_3 on triaxial stress-strain curves and ultimate failure modes are analyzed and discussed. The results show that the pH value of the chemical solution, corrosion time and the arrangement of preexisting flaws play crucial roles in the cracking behaviors of granite specimens. Type A specimens have the largest peak axial deviatoric stress, followed by Type C, Type D, and Type B specimens, respectively. It is because the decrease in the inclination of preexisting flaws induces the weakening effect due to the decrease in the shadow area along the compaction direction. Under a σ_3 of 5 MPa, the peak axial deviatoric stress drops by approximately 40.89%, 29.08%, 4.08%, and 23.53% for pH = 2, 4, 7, and 12, respectively. For intact granite (Type A) specimens, the ultimate failure mode displays a typical shear mode. The connection of two secondary cracks initiated at the tips of preexisting cracks is always the ultimate failure and crack coalescence mode for Type B specimens. The ultimate failure and crack coalescence mode of Types C and D specimens are significantly affected by pH value of the chemical solution, corrosion time and σ_3, which is different from those of Types A and B specimens due to the differences in flow distributions.

Received June 7, 2021; accepted November 8, 2021

E-mail: liuricheng@cumt.edu.cn

Keywords granites, preexisting flaws, chemical corrosion, triaxial compression, strength, cracking behavior

1 Introduction

Geothermal systems can be divided into hydrothermal geothermal system and enhanced geothermal system (EGS) based on the depth of the geothermal resources (Lu, 2018). The current EGS is commonly used for dry-hot-rocks (DHR) that refer to the dense rock matrix with no or a little fluid and are buried in a depth of 3–10 km below the surface of the earth with a temperature ranging 150°C–650°C (Lu, 2018). Compared to hydrothermal geothermal system, the EGS has the advantages of releasing more heat by opening fractures and injecting fluid into them. Chemical stimulation is a key method to increase permeability of EGS by injecting acid into the DHRs (Taron and Elsworth, 2010; Olasolo et al., 2016; Rathnaweera et al., 2020). Elevated acid concentrations have been shown to be effective in geothermal wells producing from natural fractures, by providing preferential flow paths. The chemical corrosion is commonly carried out following three steps. The first step is pre-flush using HCl to displace the formation brine away from the wellbore, then is the main flush using HCl-HF mixture to remove the damaged asperities. The final step is the over-flush using HCl, KCl, NH_4Cl solutions or freshwater to displace the none-reacted mud acid and the mud acid reaction products into the formation away from the wellbore. It has been effectively proved that the productivity of the EGS reservoir at Soultz-sous-Forêts injectivity index increased up to 35% after the treatment of chemical corrosion (Portier et al., 2019).

Over the past few decades, the chemical stimulation through laboratory tests and numerical simulations has

been systematically investigated. For instance, Feng et al. (2001) developed a new testing system for investigating the strength and micro-fracturing of granites based on the Three Gorges Project, taking into consideration of chemical corrosion. The results verified that the magnitude of decrease in strength through uniaxial compression test depends on the acidic/alkaline degree of the solution. Li et al. (2003) developed a model for chemical damage intensity of sandstones treated by different pH chemical solutions through uniaxial compression test, and the proposed model was tested and verified by laboratory experiment results. Feng et al. (2004) used the real-time CT techniques to describe the damage evolution process of sandstones subjected to chemical corrosion through triaxial compression, and the results verified that the most significant parameter to describe the damage evolution process of specimens is the CT value which corresponds to rock density at the CT scanning layer. Xie et al. (2011) analyzed the chemical degradation effect on mechanical behavior of a porous limestone through hydrostatic and triaxial compression experiments. It was indicated that the parameters that include pore collapse limit stress, elastic modulus and material cohesion were reduced resulting from the chemical degradation. Ding (2012) performed a time-dependent experiment on sandstone specimens under different pH value solutions to study the change in mass and elastic wave velocity of sandstone samples. Due to the superiority of being highly sensitive to micro void, the elastic wave velocities of specimens can be used to represent the damage degree of specimens. Zhou et al. (2016) investigated the hydro-mechanical–chemical (HMC) coupling behavior of sandstones under the condition of CO_2 storage in aquifers, and they concluded that the elastic modulus decreased with an increasing chemical reaction time. Han et al. (2016) studied the damage deterioration mechanism of sandstone specimens under coupling effects of freeze–thaw cycles and chemical corrosion conditions and proposed a damage variable based on porosity variation to quantitatively analyze the damage of the specimen. It was concluded that both freeze–thaw cycle treatment and chemical corrosion can substantially weak the mechanical behaviors of sandstone specimens. Miao et al. (2016) analyzed mechanical properties of granite specimens subjected to acidic chemical corrosion and flow rates through uniaxial and triaxial compression experiments as well as splitting tests. They concluded that the water-rock interaction with chemical corrosion depends on the ingredient of the chemical solution and the mineral components, particles, pores and cracks of rocks. The experimental results indicated that the granite has an obvious weakening trend after chemical corrosion. Qiao et al. (2017) performed uniaxial compression and real time porosity tests on sandstone specimens with distilled water and five aqueous solutions characterized by various pH values to evaluate the effect of the hydro-physical and hydro-chemical interactions on sandstones. Li et al. (2018) used nuclear magnetic resonance (NMR) system to investigate the micro damage of limestone specimens subjected to chemical corrosion and cyclic loads, and the results confirmed that chemical corrosion has a very important effect on the development of micro cracks and can accelerate the damage process of the limestone samples under cyclic loads. Luo et al. (2018) analyzed the mechanical and hydraulic properties of fractured granites under chemical stimulation using mud acid, including the change in the surface morphology of granite specimens. The results indicated that in order to improve the hydraulic properties of the fractured granites with chemical stimulation, the chemical type, reaction time and dose should be organized very carefully.

On the other hand, many works contributed to interpreting the mechanism of the cracking behavior of rocks and/or rock-like materials containing one or multiple flaws. Here, the term “flaw” is used to represent an artificial fracture. Since Bombolakis (1968) investigated the tensile wing crack from preexisting flaws through uniaxial compression test, the cracking behavior has been extensively studied in the following decades. Wong and Chau (1998) performed uniaxial compression test on a sandstone-like material, which contains two parallel inclined frictional flaws, to obtain the pattern of crack coalescence and mechanical properties of the sample. Three main modes of crack coalescences were obtained and introduced. Wong and Einstein (2008a, 2008b) experimentally studied cracking and coalescence behavior at both macroscopic and microscopic scales, using a high-speed video system, a scanning electron microscope (SEM) system and environmental scanning electron microscope (ESEM) imaging techniques. They found that the cracking process can be classified into nine crack coalescence categories. Maligno et al. (2010) developed a damage tolerance approach based on the finite element method (FEM) using three-dimensional remeshing techniques to characterize the influence of diverse factors, including crack shape, crack closure on non-planar crack development in solid and hollow shafts under mixed-mode loading. Yang and Jing (2011) investigated the mechanical and crack coalescence behavior of brittle sandstone specimens that contain a single flaw through uniaxial compression test and analyzed the evolutions of uniaxial compressive strength, Young’s modulus and peak axial strain. The results indicated that the single flaw plays an important role in deciding the magnitudes of these parameters, and these parameters are closely related to the flaw length and inclination angle. Lee and Jeon (2011) estimated crack initiation, propagation and coalescence of pre-flawed specimens under uniaxial compression tests. The results provided a reference value to understand the characteristics of crack development and crack coalescence. Zhang and Wong (2011) numerically studied cracking processes of rock-like materials with a single flaw through uniaxial compression test using parallel bonded-particle model approach (PBPMA). They reported that with increasing the uniaxial compression load, diverse new microcracks are initiated

at the tips of the flaw, which later propagated and coalesced into macrocracks and led to the ultimate damage. Wong and Li (2013) numerically investigated the coalescence of two preexisting coplanar flaws within rocks through AUTODYN as the numerical tool under compression tests. The results indicated that the coalescence pattern is significantly affected by the flaw inclination and the ligament length. Li and Wong (2013) systematically investigated the coalescence of two preexisting parallel flaws in rock-like materials subjected to a uniaxial compressive loading and obtained 11 coalescence patterns based on the numerical stimulation results. Huang et al. (2016) investigated the deformation and strength behaviors of sandstones with two preexisting flaws through triaxial compression test and numerical simulation. They found that compared to confining pressure σ_3, the arrangement of the flaw pattern has a greater influence on the rock deformation, strength and crack coalescence pattern. The diverse researchers defined the cracks observed in their experiment tests or numerical simulation differently due to various test conditions, such as flaw geometry, load path, and so on. However, they have some common characteristics. For example, the wing cracks are tensile cracks which initiated near the tips of the flaws and propagate stably toward the direction of the maximum compression. The secondary cracks initiated from the tips of the flaws and propagated coplanar with the flaws in most cases.

However, the researches on the mechanical properties and cracking behavior of pre-flawed rocks treated by chemical corrosion under triaxial compression tests are relative few. In the present study, first, a total of 128 granite specimens were prepared with different types of preexisting flaws and were treated by chemical corrosion using pH = 2, 4, 7, and 12 chemical solutions for 5 or 30 days. Then, the mechanical properties including peak strength, critical stress for crack initiation, volume dilation, and the influences of σ_3 and pH value on the peak strength of tested specimens were analyzed under triaxial compression tests. Finally, the ultimate failure and crack coalescence modes were analyzed to estimate cracking behaviors of tested specimens.

2 Experimental methods

2.1 Description of the specimens

A total of 128 cylindrical granite specimens were prepared. The main mineral components of the tested granite specimens are 49% plagioclase, 42% quartz and 6% Mica. The size was 100 mm in height and 50 mm in diameter. The geometry of the granite specimens is shown in Fig. 1 and Table 1. The behavior of rock masses is determined by the presence of discontinuities. Such discontinuities are found at any scale, from grain boundaries to joints and regional faults (Sagong and

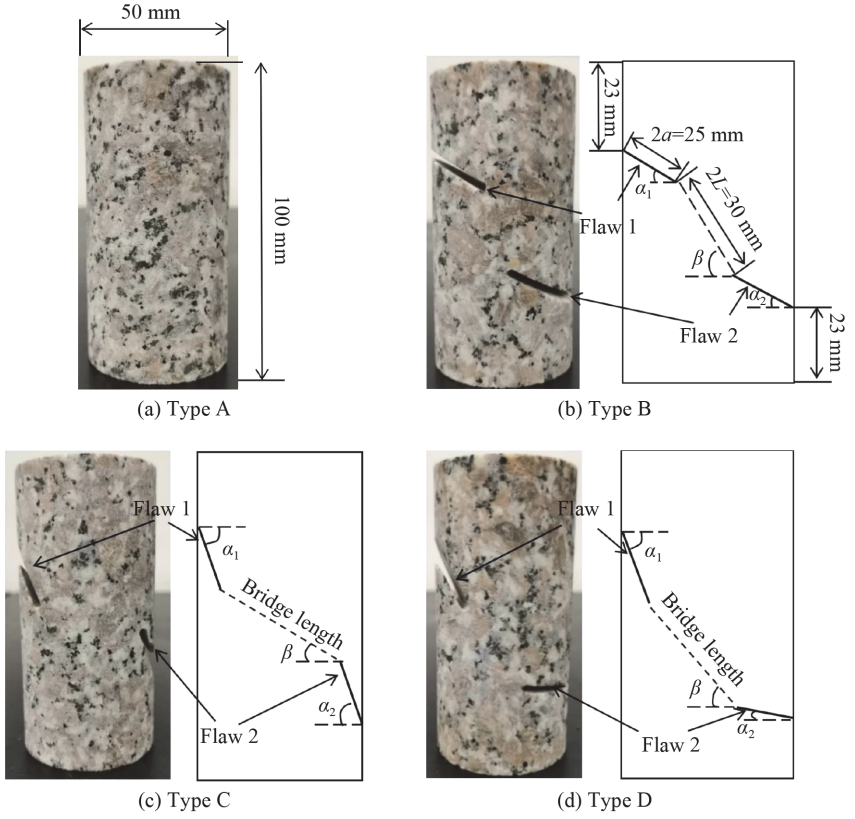

Fig. 1 Four types of tested granite specimens.

Table 1 Tested granite specimens

Type	Inclination angle of flaw 1, α_1/(°)	Inclination angle of flaw 2, α_2/(°)	Inclination angle of ligament, β/(°)	Flaw length, 2a/mm	Ligament length, 2L/mm
A	–	–	–	–	–
B	30	30	77	25	30
C	65	65	17	25	29
D	65	10	61	25	31

Bobet, 2002). When there are two flaws, they may be parallel to each other or have intersections. Two flaws parallel to each other may have a relatively low-dip or high-dip. Therefore, three types of different pre-flawed granites were used in this test. There are four types of samples. Type A is the intact sample with no preexisting flaws. Types B and C are the samples containing two relatively low-dip flaws and two relatively high-dip flaws, respectively. Type D is the sample including both relatively low-dip and relatively high-dip flaws. To reduce the effect of the end friction of the granite specimens, the length between one end of the specimens and the external flaw tips is fixed as 23 mm. The length of the flaw is fixed as 25 mm. α_1 and α_2 are the inclinations of flaw 1 and flaw 2, respectively. 2L is the length of the two internal flaw tips representing the bridge length, and β is the bridge angle.

2.2 Chemical solutions and soaking experiment

Four kinds of chemical solutions were prepared with pH = 2, pH = 4, pH = 7, and pH = 12, respectively. The solution of pH = 7 is the distilled water. Although the geothermal systems are typically treated by acid solutions (i.e., pH = 2 and/or 4), the alkaline solutions can also react with the granites. Therefore, the effect of alkaline solution (i.e., pH = 12) is considered. The solution with pH = 7 is utilized as the reference. The selections of solutions with pH = 2, 4, 7, and 12 were commonly acceptable in many previous works such as Feng et al. (2004). The acidic solutions were made by concentrated hydrochloric acid with 12 mol/L, and the alkaline solutions were made by NaOH solid. The solution containers were made of polyvinyl chloride with a geometry of 500 mm × 350 mm × 350 mm, because this material can withstand the corrosion of strong chemical solutions. The specimens were classified into 4 groups according to different pH values of chemical solutions, and then were placed into 4 containers with 32 samples in each one. The chemical solution volume was 18 L so that the chemical solution can fully cover the samples. The pH value of the chemical solution was measured using a pH pen and the value was maintained at a fixed value by adding concentrated hydrochloric acid or NaOH solid into corresponding chemical solution every day during the whole soaking phases. Since the volume of solutions is much larger than that of samples, the change in pH value during one day is controlled to be less than 0.1. The soaking experiment was carried out at a room temperature to minimize the influence of temperature on the interaction of the chemical-rock solution with tested specimens. The total soaking phases were 5 days and 30 days.

2.3 Triaxial compression test apparatus and procedure

Conventional triaxial compression tests were carried out on intact granite samples and pre-flawed granite samples based on an MTS815.02 rock mechanism testing system as shown in Fig. 2(a). The maximum axial force is 2800 kN and the maximum σ_3 is 80 MPa. The axial strain capacity measured by axial extensometer ranges from 0 to 5 mm and lateral strain capacity measured by lateral extensometer is up to 8 mm as shown in Fig. 2(b). The effect of the end friction on test results were distinctly reduced by placing two short cylindrical rigid steels on both ends of the granite samples.

The σ_3 of the triaxial tests are 0, 5, 10, and 20 MPa, respectively. The σ_3 was first applied to the specimen at a

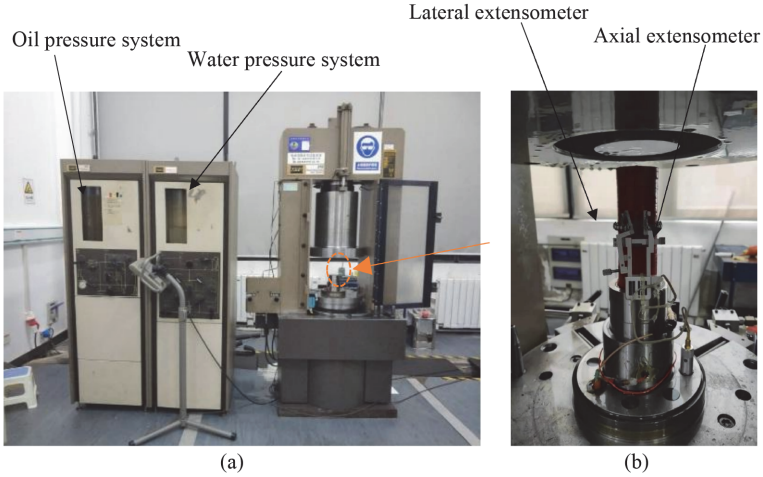

Fig. 2 (a) MTS815 rock mechanics testing system. (b) Strain measurement with extensometers.

constant rate of 0.1 MPa/s to ensure that the granite samples were under uniform hydrostatic stresses. Then, the axial deviatoric stress was applied on the surface of the samples at a 0.04 mm/min displacement rate. The magnitudes of the loading value and the displacement were recorded simultaneously during the entire conventional triaxial tests. After the soaking experiments, the gypsum was added into the preexisting flaws of pre-flawed specimens (Types B, C, and D) to avoid oil entering into the tested specimens during triaxial compressions.

3 Experimental results and analysis

3.1 Stress-strain curves

The axial deviatoric stress-strain curves for the tested samples of four different types (Types A, B, C, and D) under σ_3 of 0, 5, 10, and 20 MPa for 5 or 30 soaking days are presented in Figs. 3–6. The triaxial compressive strength of intact and pre-flawed samples increases gradually with the increase in the σ_3. The stress increases nonlinearly versus strain for all cases at the initial phase, which becomes less obvious as the σ_3 increases. It is because when the specimen was subjected to a low σ_3, a large deformation may occur due to the closure of open microcracks, yet the open microcracks were closed by the large σ_3 before the start of compression. After the stage of nonlinear deformation, the specimens deformed approximately in a linear elastic way, which represents the linear part of the stress-strain curves. Thereafter, the stress-strain curves changed to the stress hardening stage, which started at the ending point of the linear portion in the stress-strain curve named the yield point. During the stage of stress hardening, with the increment of σ_3, the obvious dilation occurs, resulting from the quick deformation in the circumferential direction. Finally, when the axial deviatoric stress reached the peak value, the stress dropped shapely with a little raise of axial strain ε_1, indicating that the granite specimens of four types subjected to different chemical solutions still showed brittle failure under triaxial compression when the σ_3 is lower than 20 MPa. Typical triaxial stress–strain curve with four stages of Type A granite specimens treated by pH = 2 chemical solution for 5 days is shown in Fig. 7.

For the intact granite specimens (Type A) with 5 or 30 soaking days under σ_3 of 0 MPa, stress drop occurred at most of cases before the peak deviatoric strength except for the specimen treated by pH = 7 solutions for 5 days as shown in Figs. 3(a) and 3(b). However, stress drop was not observed under large σ_3 such as 5, 10, and 20 MPa, owing to the restriction from the large σ_3. Table 2 lists the deformation parameters of four types of intact or pre-flawed granite specimens. Here, σ_p is the peak strength of σ_1, which equals to the axial deviatoric stress adding to the σ_3; σ_{cd} is the critical stress of volume dilation; ε_{vc} is the strain of peak ε_v value which indicates that the specimen at this point will switch from compaction-dominated to dilatancy-dominated characters; σ_{cr} is the residual strength of the tested specimen and ε_{1c} is the peak strain value at the direction of compression. During the triaxial compression tests, the oil entered into some samples such as B7-30-d and thus the tests were terminated. Therefore, these data were not recorded in Table 2. According to ε_{1c} and ε_{vc} values listed in Table 2 and Fig. 3, both ε_{1c} and ε_{vc} increase linearly with increasing σ_3 of intact granite specimens, even though the specimens have been treated by chemical corrosion for 5 or 30 soaking days. Compared to the post-peak stress-strain curves of Fig. 3(a) with Fig. 3(b) for the case with a σ_3 of 0 MPa, the intact specimens with 30 soaking days have more significant stress fluctuations due to the longer time of the chemical corrosion, which could not be found under a large σ_3. It can be described that the hydrogen ions in the acid solutions (i.e., pH = 2 and pH = 4) react with the SiO_2 of granite samples, and the hydroxide ions in the alkaline solution (pH = 12) can also react with the SiO_2 of granite specimens (Miao et al., 2016). With the increasement of the corrosion time, the ions in the solutions more fully reacted with the tested samples. The stress-strain curves of Fig. 3(b) show more obvious concaved downward trends than those in Fig. 3(a), especially for the specimens soaked in the solution of pH = 2. It can be concluded that the initial compressive phase can be prolonged by the chemical corrosion. When σ_3 equals to 20 MPa, the deformation of the intact granite specimens with 5 or 30 soaking days treated by different chemical solutions all exhibit obvious yielding platforms as shown in Figs. 3(g) and 3(h). The σ_3 of 20 MPa can be defined as the transition σ_3 of intact granite samples. The peak axial deviatoric stress of the intact granite specimens under 5 soaking days remains roughly the same, yet the chemical solution has distinct influence on the reduction of the peak axial deviatoric stress under 30 soaking days. For example, at the σ_3 of 5 MPa, the peak axial deviatoric stresses drop in magnitude, which is defined as the ratio of the difference of the peak axial deviatoric stresses between the specimens under 5 soaking days and 30 soaking days, by approximately 40.89%, 29.08%, 4.08%, and 23.53% for pH = 2, 4, 7, and 12, respectively. The larger stress fluctuation can be found in the intact granite samples treated with longer corrosion time. With increasement of corrosion time, the ions in acid or alkaline solutions can fully react with samples by inserting into the pores. However, the pores are randomly distributed, resulting in the random change in mechanical behaviors such as stress. With the increasement of confining pressure, the porosity decreases and the randomness of rock-solution reaction decreases. As a result, the stress fluctuates more significantly for a lower confining pressure.

Figures 4–6 display typical stress-strain curves of pre-flawed granite samples of Types B, C, and D,

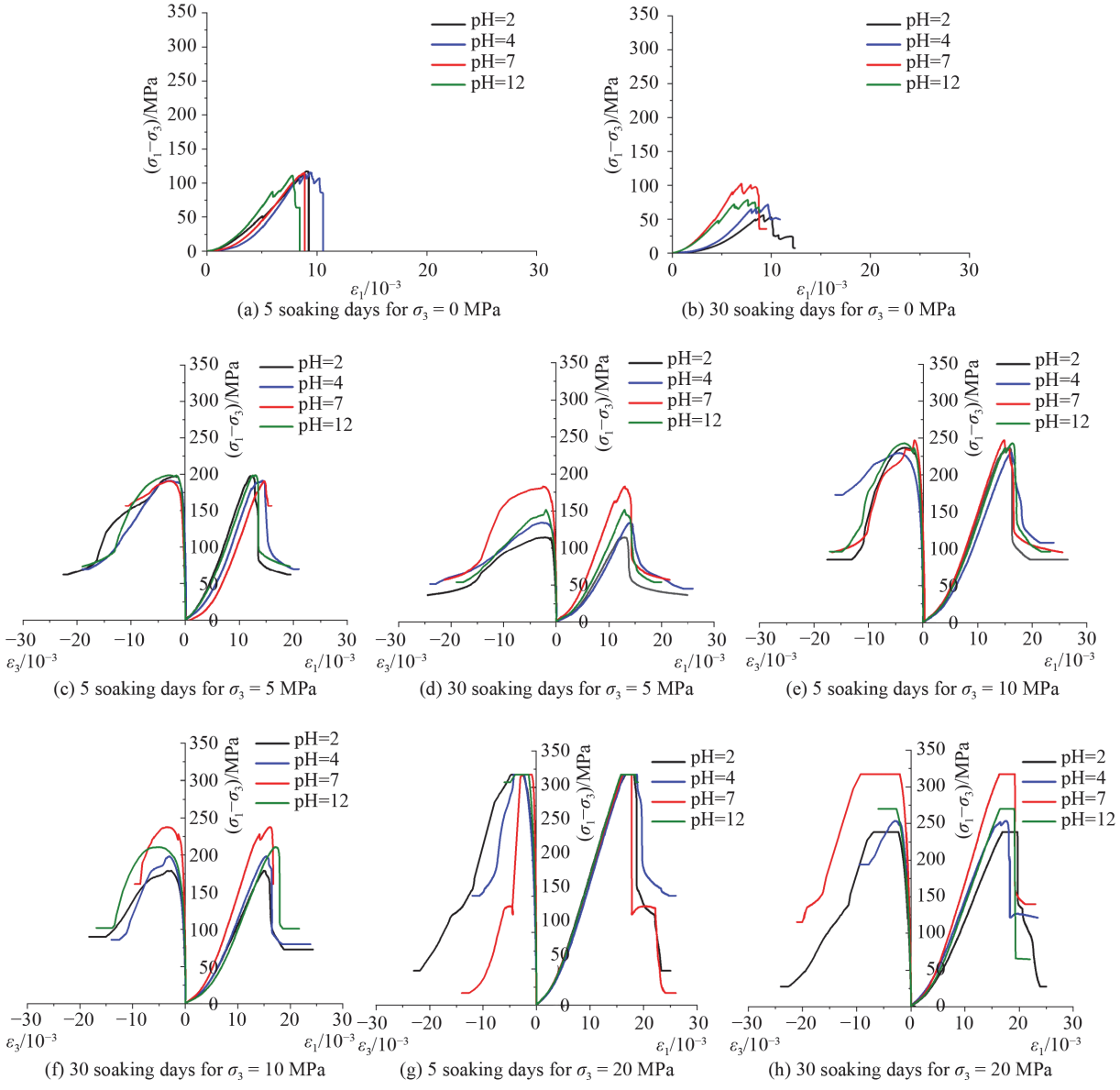

Fig. 3 Triaxial stress–strain curves of Type A granite specimens under different confining pressures and soaking days.

respectively. Compared with intact specimens, the peak axial deviatoric stresses of Type C with two preexisting high-dip flaws (Fig. 5, Table 2) have least difference with these found in intact samples (Type A), followed by Type D with composite high- and low-dip flaws, and finally by Type B with two preexisting low-dip flaws. The decrease in the inclination of preexisting flaws induces the weakening effect due to the decrease in the shadow area along the direction of compaction. The Type B granite samples failed at a strain of approximately 0.4%–1.4%, which were smaller than those of Type D and Type C with 0.6%–2.5% and 0.7%–1.9%, respectively. The failure strain of intact granite specimens increases with increasing σ_3, however, for pre-flawed samples of Types B, C, and D, the failure strain increases nonlinearly with increasing σ_3, which is dependent on the coalescence of the pre-flawed samples under different σ_3. Similar to intact samples, compared with the peak axial deviatoric stress value of pre-flawed specimens for Types B, C, and D for 5 soaking days (Figs. 4–6 and Table 2), the peak axial deviatoric stress comes down a lot when the pre-flawed samples soaked in the chemical solutions for 30 days, and the smaller (pH = 2, 4) or larger (pH = 12) the pH value, the greater the decrease in the peak axial deviatoric stress. The chemical solutions have a great influence on the peak strength of the intact and pre-flawed granite samples under 30 soaking days, yet the strength of specimens treated by chemical corrosion for 5 days does not change significantly. For pre-flawed specimens soaked in different chemical solutions with the same geometry of flaws, the corresponding stress-strain curves presented the similar trends. This indicates that the arrangements of flaws play a more crucial role on the deformations of the tested samples than the chemical

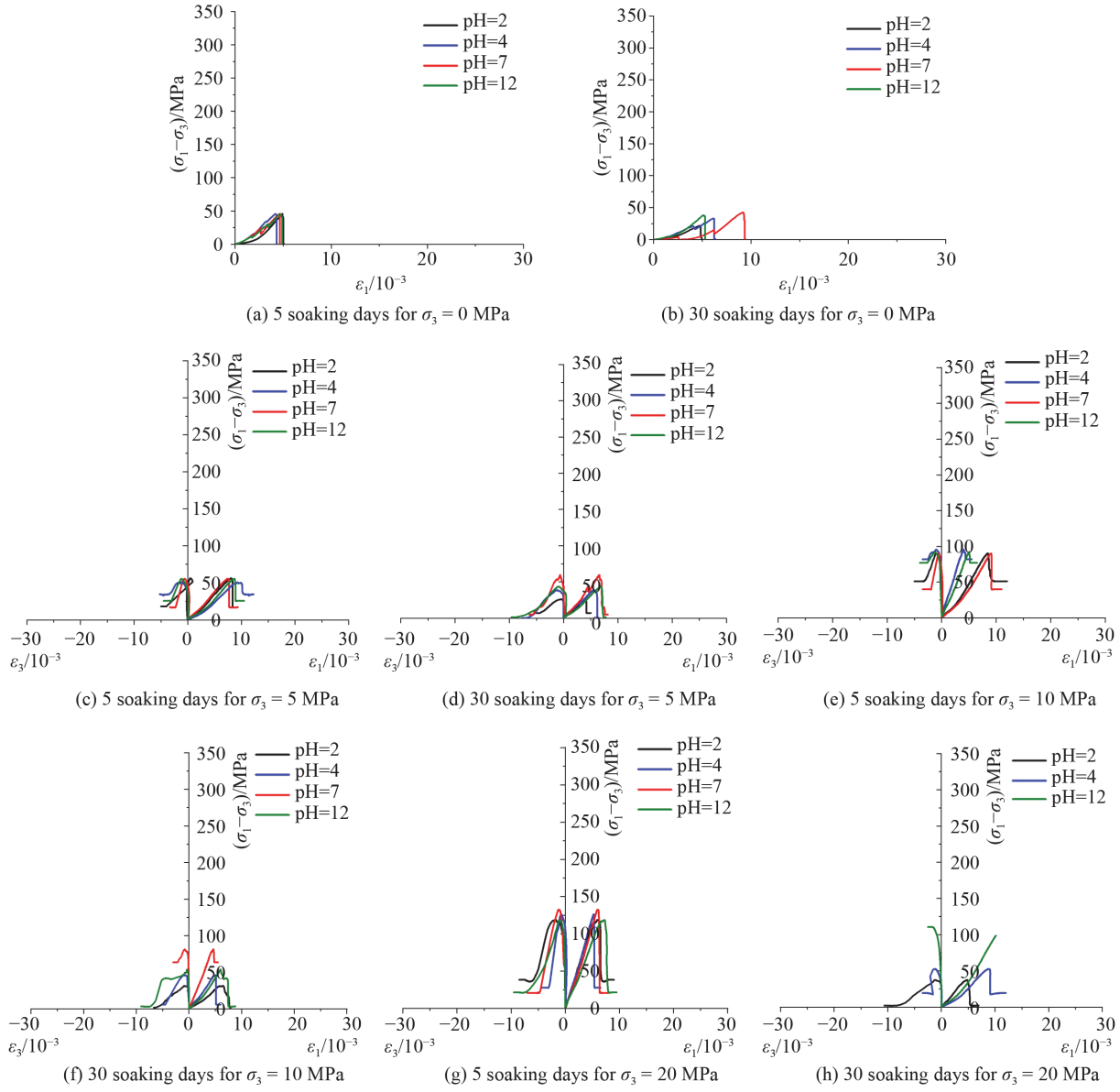

(a) 5 soaking days for σ_3 = 0 MPa

(b) 30 soaking days for σ_3 = 0 MPa

(c) 5 soaking days for σ_3 = 5 MPa

(d) 30 soaking days for σ_3 = 5 MPa

(e) 5 soaking days for σ_3 = 10 MPa

(f) 30 soaking days for σ_3 = 10 MPa

(g) 5 soaking days for σ_3 = 20 MPa

(h) 30 soaking days for σ_3 = 20 MPa

Fig. 4 Typical triaxial stress–strain curves of Type B granite specimens under different confining pressures and soaking days.

corrosion and σ_3. The residual part of Type D specimens in the stress-strain curves reveals that the residual stress increases with increasing deformation to a small extent under large σ_3 (i.e., σ_3 = 5, 10, and 20 MPa) in most cases, which is different for the Types A, B, and C. Some stress-strain curves of pre-flawed samples show double-peak stresses, e.g., specimens in Fig. 4(d) with pH = 7, in Fig. 5(f) with pH = 2 and in Fig. 6(h) with pH = 4. In addition, there are some specimens with a treble-peak stress in Type D, e.g., specimen in Fig. 6(f) with pH = 12. The stress-strain curves are approximately linear again after the strength reached the first valley point, yet the slope of the curve in the second or third quasi-elastic phase is obviously lower than that in the first quasi-elastic phase, indicating that the specimens have been damaged in the first quasi-elastic phase. It is reasonable that the peak axial stress of intact samples (i.e., Type A) is larger than that of flawed samples (i.e., Types B, C, and D), due to the existence of cracks. Since the inclination between the flaws and the axial direction of the samples increases for specimens of Types C, D, and B, the peak axial stress will accordingly decrease. Therefore, for the cases with the same pH value and soaking days, the peak axial stress of Type A is the largest, followed by Type C, Type D, and Type B.

3.2 Analyses of the critical stress for crack initiation and volume dilation

The crack initiation stress σ_{ci} is defined as the ending point of the linear portion in the stress-strain curves, in which the cracks begin to initiate and propagate. The

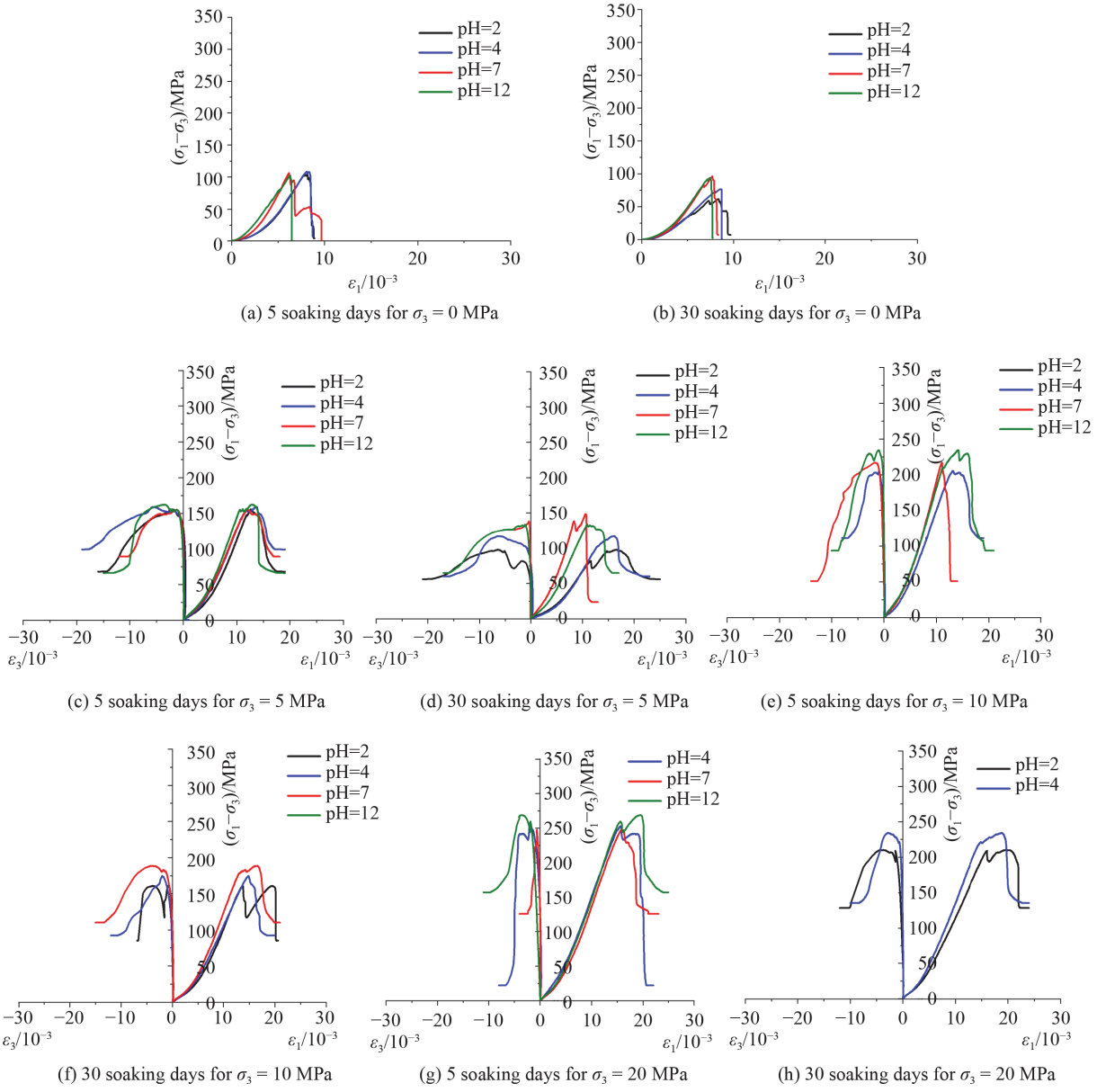

(a) 5 soaking days for σ_3 = 0 MPa (b) 30 soaking days for σ_3 = 0 MPa

(c) 5 soaking days for σ_3 = 5 MPa (d) 30 soaking days for σ_3 = 5 MPa (e) 5 soaking days for σ_3 = 10 MPa

(f) 30 soaking days for σ_3 = 10 MPa (g) 5 soaking days for σ_3 = 20 MPa (h) 30 soaking days for σ_3 = 20 MPa

Fig. 5 Typical triaxial stress–strain curves of Type C granite specimens under different confining pressures and soaking days.

critical stress of volume dilation σ_{cd} represents that the deformation of the tested samples switches from compaction-dominated to dilation-dominated characters. Both σ_{ci} and σ_{cd} can be determined by analyzing the volumetric strain of the tested samples. The volumetric strain ε_v can be divided into two parts. One is the result of the crack closure and the initiation or propagation of the new cracks, which is defined as the crack-induced volumetric strain ε_v^c. The other is the elastic volumetric strain ε_v^e, in which the strain is induced by the elastic deformation of the rock material. Therefore, the value of the crack-induced volumetric strain can be calculated using Eq. (1) and the volumetric strain can be obtained by Eq. (2). The elastic volumetric strain ε_v^e can be derived from Eq. (3):

$$\varepsilon_v^c \approx \varepsilon_v - \varepsilon_{v,}^e \quad (1)$$

$$\varepsilon_v^c \approx \varepsilon_v - \varepsilon_v^e, \quad (2)$$

$$\varepsilon_v^e = (1-2\mu)(\sigma_1 + 2\sigma_3)/E, \quad (3)$$

where E is the elastic modulus and μ is the Poisson ratio of intact rock.

As mentioned above, the arrangements of preexisting flaws play a more crucial role on the deformations of tested samples than the chemical corrosion and σ_{cd} pressure. Therefore, we chose the evolutions of typical deviatoric stress $(\sigma_1-\sigma_3)$, ε_v and ε_v^c versus axial strain ε_1 of tested specimens soaked at pH = 2 chemical solutions for 30 days under a σ_3 of 5 MPa as an example as shown in Fig. 8. The deformation of the tested granite samples can be divided into five phases. The first is the phase I corresponding to the part of curves from point 0 to point

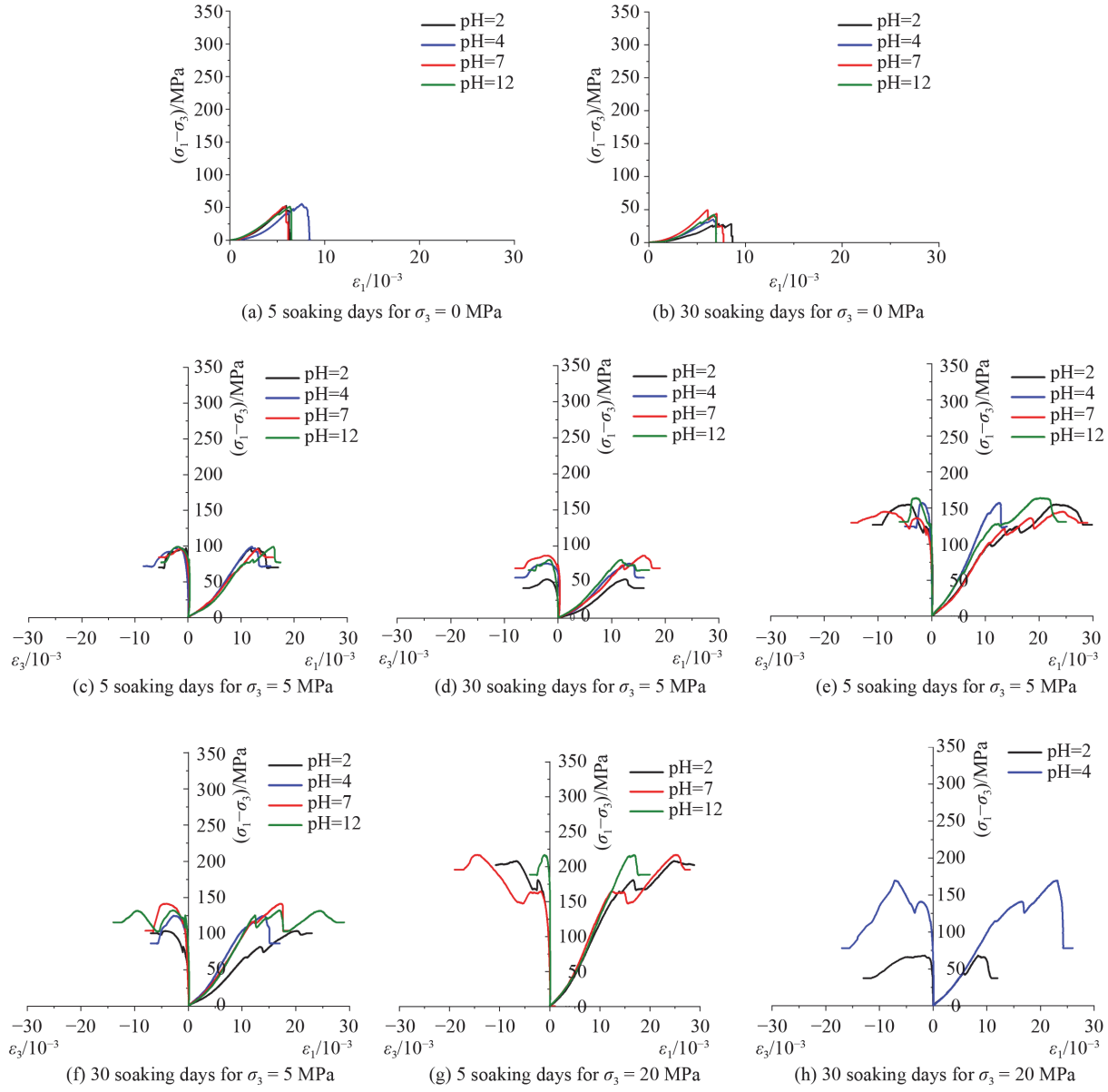

(a) 5 soaking days for σ_3 = 0 MPa (b) 30 soaking days for σ_3 = 0 MPa

(c) 5 soaking days for σ_3 = 5 MPa (d) 30 soaking days for σ_3 = 5 MPa (e) 5 soaking days for σ_3 = 5 MPa

(f) 30 soaking days for σ_3 = 5 MPa (g) 5 soaking days for σ_3 = 20 MPa (h) 30 soaking days for σ_3 = 20 MPa

Fig. 6 Typical triaxial stress–strain curves of Type D granite specimens under different confining pressures and soaking days.

A, in which the closure of the cracks mainly occurs, and shows a nonlinear variation trend. The second phase (phase II) is the segment between points A and B named as the elastic deformation phase, in which the value of the ε_v^c versus ε_1 remains constant or increases slightly. However, the value of ε_v versus ε_1 still increase linearly, which means that the tested samples are under the state of compaction. The third phase (phase III) is the stable crack growth part corresponding to the segment between points B and C. The value of the ε_v^c starts to decrease with increasing ε_1, but the value of ε_v still increases in a nonlinear way versus ε_1. This indicates that although the tested specimens have come into the phase of the stable crack growth, they are still in compaction-dominated phase. Subsequently, the phase IV (the segment between points C and D) refers to the phase of initiation and development

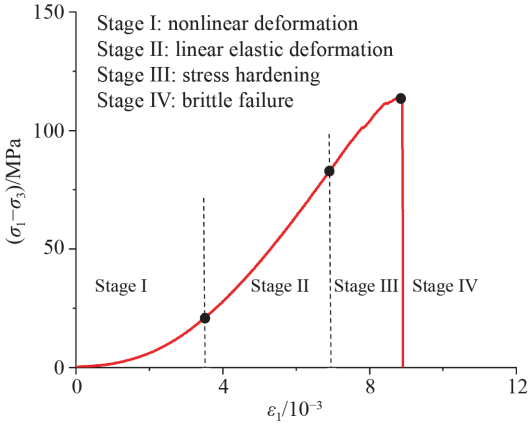

Fig. 7 Typical triaxial stress–strain curve with four stages of Type A granite specimens treated by pH = 2 chemical solution for 5 days.

Table 2 Physical and mechanical properties of tested granite specimens

Specimen	Fracture mode	σ_3/MPa	Soaking days	pH value	σ_p/MPa	σ_{cd}/MPa	σ_{cr}/MPa	ε_{vc}/(×10^3)	ε_{1c}/(×10^3)
A_2-5-a	A	0	5	2	117.15		0		9.25
A_2-5-b	A	5	5	2	202.52	186.91	58.74	9.37	12.03
A_2-5-c	A	10	5	2	246.48	221.75	70.43	10.64	15.78
A_2-5-d	A	20	5	2	337.53	312.26	48.38	11.83	18.23
A_2-30-a	A	0	30	2	55.61		12.38		9.21
A_2-30-b	A	5	30	2	119.58	113.63	36.70	10.02	13.00
A_2-30-c	A	10	30	2	188.57	161.42	51.92	10.84	14.96
A_2-30-d	A	20	30	2	258.15	236.17	27.51	12.50	19.66
A_4-5-a	A	0	5	4	111.02		0		9.39
A_4-5-b	A	5	5	4	196.34	186.15	60.70	10.07	14.23
A_4-5-c	A	10	5	4	239.45	191.24	105.80	11.22	16.06
A_4-5-d	A	20	5	4	337.53	317.03	151.33	11.96	18.80
A_4-30-a	A	0	30	4	71.43		49.48		9.63
A_4-30-b	A	5	30	4	139.41	121.24	45.18	10.05	14.21
A_4-30-c	A	10	30	4	208.03	173.20	65.61	11.41	15.41
A_4-30-d	A	20	30	4	272.68	248.24	121.32	12.63	17.66
A_7-5-a	A	0	5	7	114.92		0		8.87
A_7-5-b	A	5	5	7	195.77	174.86	156.63	11.14	14.61
A_7-5-c	A	10	5	7	256.83	235.43	94.89	12.04	14.88
A_7-5-d	A	20	5	7	337.53	317.53	20.76	14.54	17.76
A_7-30-a	A	0	30	7	102.35		35.66		6.97
A_7-30-b	A	5	30	7	188.02	165.58	57.01	9.78	13.08
A_7-30-c	A	10	30	7	247.70	225.88	161.17	11.59	16.17
A_7-30-d	A	20	30	7	347.53	313.18	142.23	12.44	19.17
A_{12}-5-a	A	0	5	12	111.41		0		7.78
A_{12}-5-b	A	5	5	12	203.83	187.08	73.49	9.84	12.92
A_{12}-5-c	A	10	5	12	252.98	232.24	101.23	11.93	16.31
A_{12}-5-d	A	20	5	12	337.53	317.53	306.93	13.04	18.45
A_{12}-30-a	A	0	30	12	78.53		59.51		7.58
A_{12}-30-b	A	5	30	12	156.49	132.00	53.86	9.67	13.02
A_{12}-30-c	A	10	30	12	220.98	177.55	101.49	11.91	17.15
A_{12}-30-d	A	20	30	12	289.90	257.50	57.74	19.91	19.08
B_2-5-a	B	0	5	2	45.76		0		4.93
B_2-5-b	B	5	5	2	61.25	51.41	17.39	3.36	8.00
B_2-5-c	B	10	5	2	100.25	86.38	50.88	6.59	8.46
B_2-5-d	B	20	5	2	138.10	106.49	48.82	10.13	5.92
B_2-30-a	B	0	30	2	21.55		0		4.70
B_2-30-b	B	5	30	2	31.34	25.49	10.66	3.49	3.97
B_2-30-c	B	10	30	2	41.15	31.00	1.78	3.63	6.46
B_2-30-d	B	20	30	2	57.64	34.48	2.29	5.11	4.80
B_4-5-a	B	0	5	4	45.60		0		4.17
B_4-5-b	B	5	5	4	60.64	54.51	18.82	3.02	7.49
B_4-5-c	B	10	5	4	105.66	81.92	89.99	4.46	4.03

(*continued*)

Specimen	Fracture mode	σ_3/MPa	Soaking days	pH value	σ_p/MPa	σ_{cd}/MPa	σ_{cr}/MPa	$\varepsilon_{vc}/(\times10^3)$	$\varepsilon_{1c}/(\times10^3)$
B_4-5-d	B	20	5	4	145.20	111.28	23.87	6.35	5.25
B_4-30-a	B	0	30	4	33.08		0		6.15
B_4-30-b	B	5	30	4	43.91	33.81	5.79	3.91	5.59
B_4-30-c	B	10	30	4	55.80	44.78	6.06	4.42	5.03
B_4-30-d	B	20	30	4	72.58	50.33	20.14	6.60	8.74
B_7-5-a	B	0	5	7	45.88		0		4.63
B_7-5-b	B	5	5	7	55.68	46.03	34.69	4.04	9.34
B_7-5-c	B	10	5	7	100.22	88.90	40.94	7.21	9.05
B_7-5-d	B	20	5	7	152.41	123.34	20.78	7.95	6.07
B_7-30-a	B	0	30	7	42.63		0		9.19
B_7-30-b	B	5	30	7	64.72	56.69	14.46	3.77	6.57
B_7-30-c	B	10	30	7	91.19	76.32	66.57	5.28	4.65
B_{12}-5-a	B	0	5	12	44.92		0		4.72
B_{12}-5-b	B	5	5	12	60.37	50.44	26.57	3.36	8.65
B_{12}-5-c	B	10	5	12	102.26	79.13	86.52	5.24	5.03
B_{12}-5-d	B	20	5	12	138.47	114.27	22.85	6.61	7.24
B_{12}-30-a	B	0	30	12	37.90		0		5.07
B_{12}-30-b	B	5	30	12	48.45	34.40	6.18	5.37	6.89
B_{12}-30-c	B	10	30	12	63.99	52.50	3.59	6.09	6.00
B_{12}-30-d	B	20	30	12	130.60	100.01	100.42	8.54	11.44
C_2-5-a	C	0	5	2	103.48		0		7.99
C_2-5-b	C	5	5	2	160.71	135.38	68.16	10.87	12.86
C_2-30-a	C	0	30	2	61.79		0		8.35
C_2-30-b	C	5	30	2	102.60	73.70	56.40	9.21	16.53
C_2-30-c	C	10	30	2	170.08	153.98	85.70	12.91	13.72
C_2-30-d	C	20	30	2	229.72	202.10	128.51	13.85	19.56
C_4-5-a	C	0	5	4	107.94		0		8.12
C_4-5-b	C	5	5	4	164.03	135.93	99.19	9.82	13.69
C_4-5-c	C	10	5	4	215.19	201.51	111.35	11.24	13.18
C_4-5-d	C	20	5	4	272.36	243.60	22.04	11.39	15.65
C_4-30-a	C	0	30	4	76.59		0		8.59
C_4-30-b	C	5	30	4	121.90	91.81	60.07	11.38	16.13
C_4-30-c	C	10	30	4	183.84	162.15	92.65	11.05	14.84
C_4-30-d	C	20	30	4	254.50	228.00	135.59	14.05	18.78
C_7-5-a	C	0	5	7	106.45		0		6.19
C_7-5-b	C	5	5	7	160.41	148.65	89.29	8.71	12.00
C_7-5-c	C	10	5	7	227.24	188.83	51.01	10.04	11.05
C_7-5-d	C	20	5	7	267.85	199.46	126.27	16.31	15.74
C_7-30-a	C	0	30	7	96.10		0		7.70
C_7-30-b	C	5	30	7	158.35	137.24	23.63	7.63	10.53
C_7-30-c	C	10	30	7	198.34	181.15	110.57	10.88	16.65
C_{12}-5-a	C	0	5	12	102.45		0		6.29
C_{12}-5-b	C	5	5	12	167.43	146.06	66.31	8.77	12.75
C_{12}-5-c	C	10	5	12	244.52	232.36	100.34	12.15	14.17

(*continued*)

Specimen	Fracture mode	σ_3/MPa	Soaking days	pH value	σ_p/MPa	σ_{cd}/MPa	σ_{cr}/MPa	$\varepsilon_{vc}/(\times10^3)$	$\varepsilon_{1c}/(\times10^3)$
C_{12}-5-d	C	20	5	12	289.32	263.85	156.63	12.98	19.50
C_{12}-30-a	C	0	30	12	93.95		0		7.41
C_{12}-30-b	C	5	30	12	137.67	127.53	64.81	8.74	10.96
D_2-5-a	D	0	5	2	52.35		0		5.94
D_2-5-b	D	5	5	2	103.28	97.01	70.51	11.29	14.02
D_2-5-c	D	10	5	2	164.83	150.07	126.73	14.70	23.21
D_2-5-d	D	20	5	2	228.17	185.50	202.36	12.50	24.81
D_2-30-a	D	0	30	2	27.99		0		7.24
D_2-30-b	D	5	30	2	58.59	51.43	43.74	9.05	12.49
D_2-30-c	D	10	30	2	110.68	96.57	99.74	13.22	20.13
D_4-5-a	D	0	5	4	54.20		0		7.58
D_4-5-b	D	5	5	4	104.12	96.09	71.81	9.05	12.04
D_4-5-c	D	10	5	4	167.19	151.84	125.93	9.56	12.47
D_4-30-a	D	0	30	4	34.89		0		6.67
D_4-30-b	D	5	30	4	80.79	69.53	56.24	10.68	13.36
D_7-5-a	D	0	5	7	51.57		0		5.82
D_7-5-b	D	5	5	7	100.56	88.77	84.30	9.02	13.15
D_7-5-c	D	10	5	7	154.72	129.49	129.61	11.03	24.43
D_7-5-d	D	20	5	7	237.14	155.62	195.79	13.59	25.18
D_7-30-a	D	0	30	7	49.36		0		6.07
D_7-30-b	D	5	30	7	91.68	78.36	69.20	11.29	15.88
D_7-30-c	D	10	30	7	151.07	130.61	103.37	13.11	17.08
D_{12}-5-a	D	0	5	12	51.23				6.29
D_{12}-5-b	D	5	5	12	103.73	92.33	77.13	13.59	16.11
D_{12}-5-c	D	10	5	12	173.44	131.16	130.84	14.66	20.27
D_{12}-5-d	D	20	5	12	236.47	215.16	187.94	14.85	16.83
D_{12}-30-a	D	0	30	12	42.34		0		6.76
D_{12}-30-b	D	5	30	12	87.68	79.49	67.29	8.67	22.03
D_{12}-30-c	D	10	30	12	135.13	121.68	115.67	12.65	16.94

of macroscale failure. The value of the ε_v starts to decrease accompanied with a quick drop of ε_v^c. It is indicated that the deformation of tested specimens comes into the dilation-dominated phase. Finally, the last phase (phase V) is the post-peak failure (the segment after point D), in which the value of ε_v and the ε_v^c all decrease sharply with increasing ε_1, resulting in the ultimate failure of tested specimens.

Besides, an interesting phenomenon can be found in Fig. 8(c) that both ε_v and ε_v^c decrease simultaneously right after the axial deviatoric stress reaches the point B, which represents the first peak point in this type of curves. Then the stress-strain curve presents quasi-elastic trend again until the deviatoric stress reaches the point C (the second peak point), which can be explained that the newly cracks initiated at the phase II and propagate slowly during the phase III.

4 Strength behavior of intact and pre-flawed granite specimens

4.1 Influence of σ_{cd} on strength parameters in accordance with Mohr-Coulomb criterion

To investigate the influence of the σ_3 on the σ_p and the σ_{cd}, linear Mohr-Coulomb criterion as shown in Eq. (4) is adopted:

$$\sigma_p = q\sigma_3 + \sigma_0 = \frac{1+\sin\varphi}{1-\sin\varphi}\sigma_3 + \frac{2C\cos\varphi}{1-\sin\varphi}, \tag{4}$$

where σ_p equals to the summation of the σ_3 and the axial deviatoric stress; q and σ_0 are the material parameters correlating to the cohesion C and the internal friction angle φ. Eq. (4) can be deduced to the following Eqs. (5) and (6):

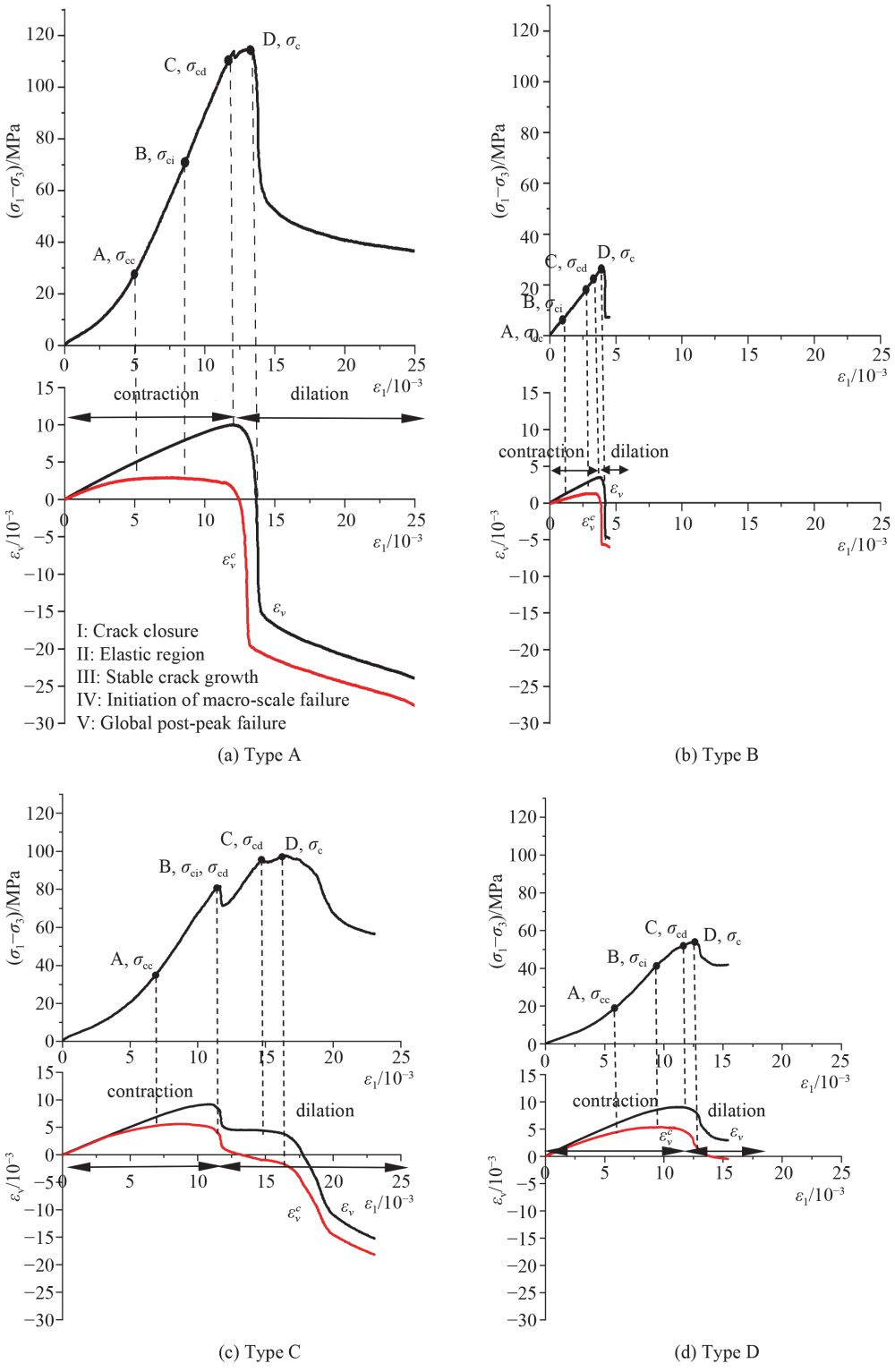

Fig. 8 Typical deviatoric stress versus axial strain curves, and corresponding volumetric strain versus axial strain curves. The samples are treated with pH =2 chemical solution for 30 days under a confining pressure of 5 MPa.

$$\varphi = \arcsin\left(\frac{q-1}{q+1}\right), \tag{5}$$

$$C = \frac{\sigma_0(1-\sin\varphi)}{2\cos\varphi}. \tag{6}$$

On the basis of Eqs. (5) and (6), the relationships among σ_p, σ_{cd} and σ_3 for specimens soaked in different chemical

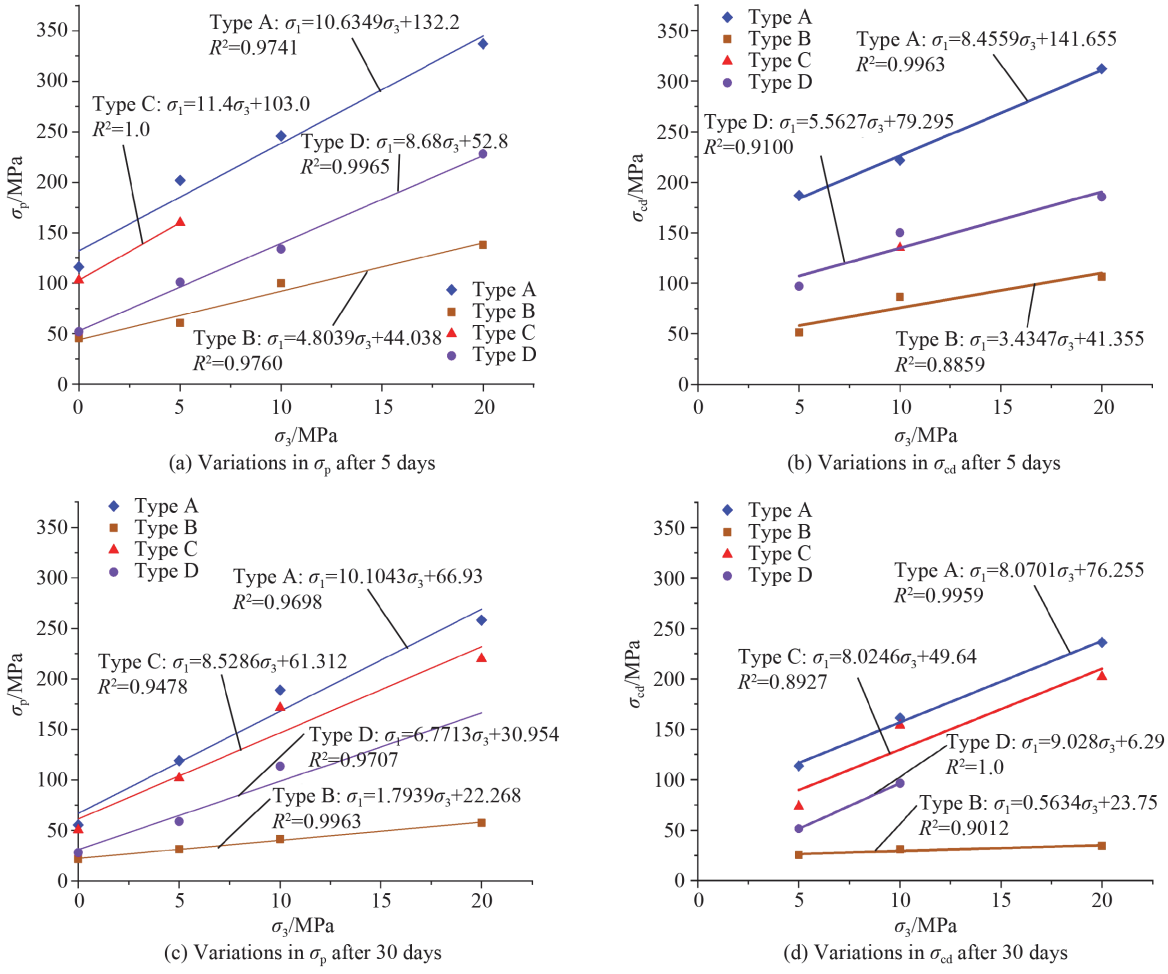

Fig. 9 Variations in peak axial stress σ_p and σ_{cd} versus confining pressure σ_3 varying from 0 to 20 MPa. The samples are treated with pH=2 chemical solution for 5 and 30 soaking days, respectively.

solutions for 5 or 30 days are shown in Figs. 9–12, and parameters calculated by the linear Mohr-Coulomb criterion are listed in Table 3. The linear regression coefficients R^2 = 0.9220–0.9978 and R^2 = 0.8088–0.9998 for σ_p and σ_{cd}, respectively. The σ_{cd} of the intact granite specimens treated by different chemical solutions for 5 or 30 days ranges from 9.21 to 19.90 MPa, which is lower than corresponding C_p value of these specimens that ranges from 13.42 to 24.52 MPa. Similar to the relationship between C_{cd} and C_p of intact specimens, the magnitudes of these parameters for Types B, C and D samples show the same trend with the intact specimens. The values of φ_p for the intact granite specimens are between 56.33° and 58.60°, which is larger than φ_{cd} ranging from 52.58° to 55.82°. The φ_p is larger than φ_{cd} in most cases, except for some cases for Type D. This may be due to that the failure modes of Types A, B and C are simpler than those of Type D samples. Types A and C are relatively the same, and the failure mode of Type B shows coalescence between the two flaws. However, various failure modes can be found in Type D samples.

Table 3 shows that the C_p value of specimens soaked for 5 days is larger than that of specimens soaked for 30 days, yet the effect of corrosion time on the values of C_{cd}, φ_p and φ_{cd} are less evident. For intact granite specimens treated by different chemical solutions for 30 days, the values of C_p and C_{cd} are largest at pH = 7, followed by pH = 12, pH = 4, and finally by pH = 2. However, the relationships do not hold on among the pre-flawed specimens. For example, the value of C_p in Type B is 10.40 MPa for pH = 4, yet the value of C_p is 9.47 MPa for pH = 7. The effect of pH value on the internal friction angles φ_p and φ_{cd} is not obvious. Therefore, the values of C_p, C_{cd}, φ_p, and φ_{cd} significantly depend on the arrangement of preexisting flaws, followed by the time of the corrosion and pH value of the chemical solution.

4.2 Influence of pH value on peak strength of intact and pre-flawed tested granite specimens

As shown in Figs. 13(a), 13(c), 13(e), 13(g) and Table 3, the specimens are treated by different chemical solutions (pH = 2, 4, 7, and 12) for 5 soaking days. When the fracture type remains the same, the peak strength σ_p remains constant with different pH values. However, when the granite samples are treated by different pH values for 30 days (Figs. 13(b), 13(d), 13(f), and 13(h); Table

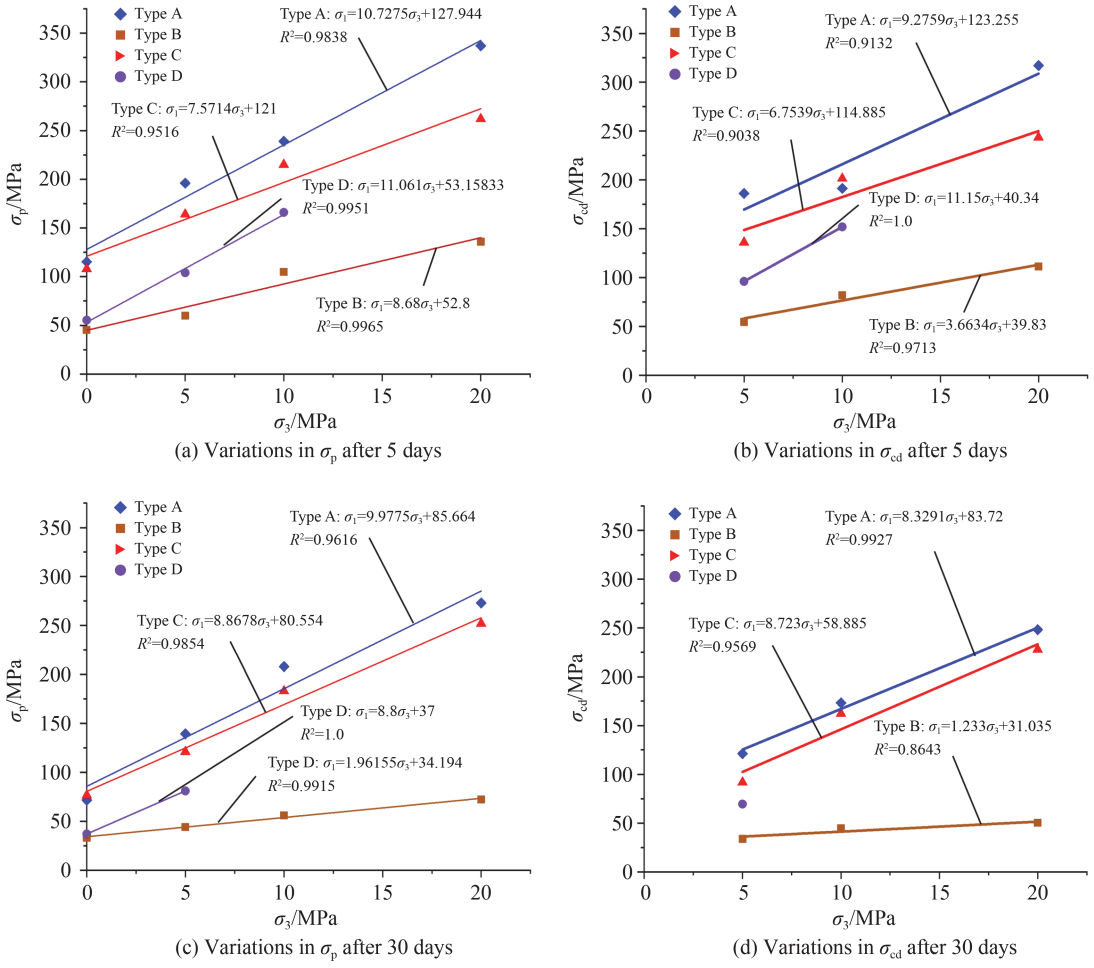

Fig. 10 Variations in peak axial stress σ_p and σ_{cd} versus confining pressure σ_3 varying from 0 to 20 MPa. The samples are treated with pH=4 chemical solution for 5 and 30 soaking days, respectively.

3), the peak strength σ_p is sensitive to the pH value of the chemical solutions. The largest drop of σ_p occurred at the chemical solution of pH = 2, followed by pH = 4, pH = 12, and finally pH = 7. This indicates that the H^+ ions of pH = 2 and pH = 4 and OH^- ions of pH = 12 chemical solutions effectively reacted with the minerals of the tested samples, resulting in generation of new cracks. The new cracks propagated and connected with other cracks or original flaws, eventually leading to decreases in σ_p.

The variation in peak axial stress is similar to that of Miao et al. (2016), which can be described that the smaller the pH value, the greater the decrease in the peak axial stress. The peak axial stresses of four different types samples show the similar variation trend with the findings discovered by Huang et al. (2016). It can be described that the peak axial deviatoric stresses of Type C with two preexisting relatively high-dip flaws have the least difference from those of Type A, followed by Type B with relatively low-dip flaws and Type D with both relatively low-dip and relatively high-dip flaws. Different from their studies, the effects of chemical solution and corrosion time are analyzed in this study.

Compared with previous studies, pre-flawed granites treated by chemical corrosion were utilized to carry out triaxial compression tests to study the mechanical behaviors in the present study. The new findings are that when the granite samples are treated by different pH values for 30 days, the σ_p is sensitive to the pH value of the chemical solutions. The largest drop of σ_p occurred at the chemical solution of pH = 2, followed by pH = 4, pH = 12, and finally pH = 7. The peak axial deviatoric stresses of Type C with two preexisting relatively high-dip flaws have the least difference from those of Type A, followed by Type B with relatively low-dip flaws and Type D with both relatively low-dip and relatively high-dip flaws specimens. The arrangements of preexisting flaws play a more crucial role on the deformations of tested samples than the chemical corrosion and confining pressure.

5 Analysis of ultimate failure mode and cracking behaviors

To analyze the failure mode of granite samples with a preexisting flaw under compression test, five different crack types were identified based on the time sequence of

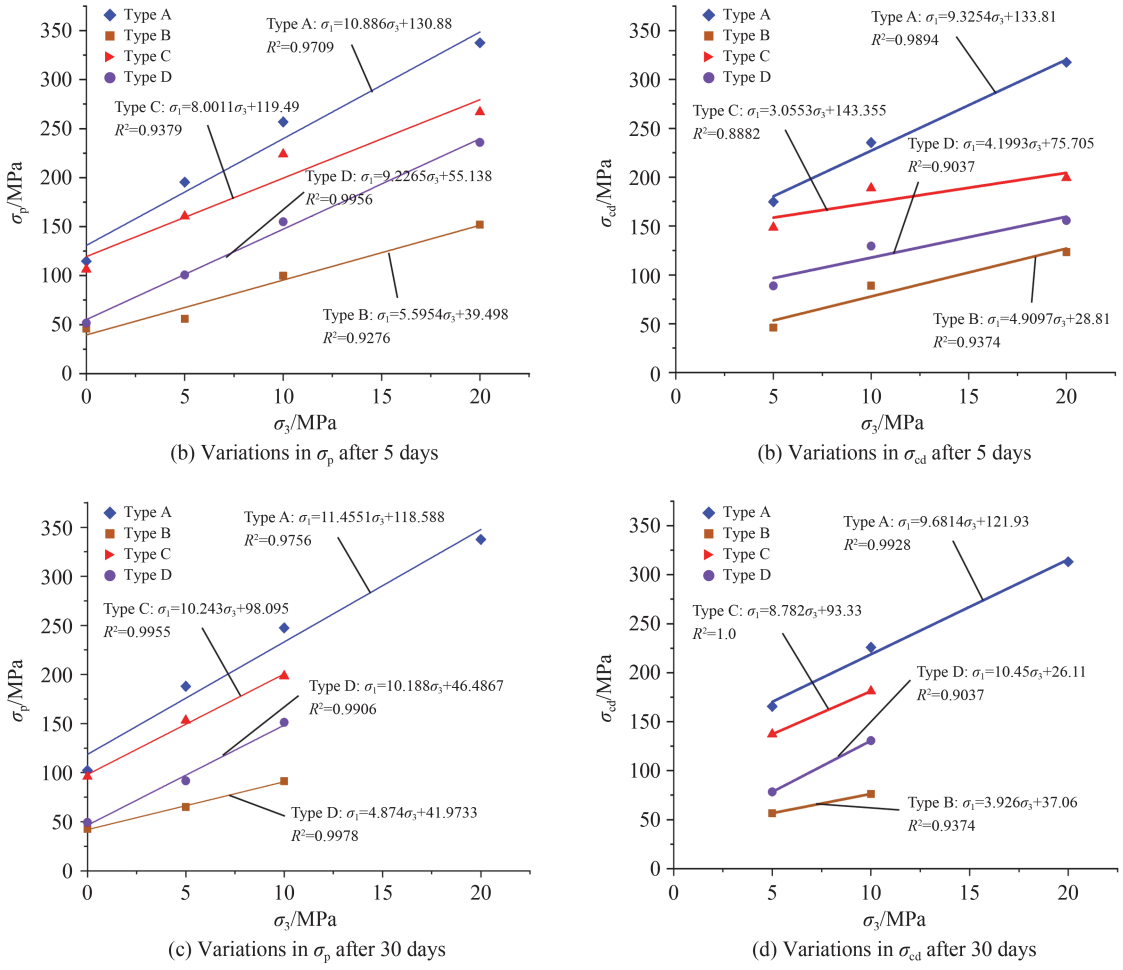

Fig. 11 Variations in peak axial stress σ_p and σ_{cd} versus confining pressure σ_3 varying from 0 to 20 MPa. The samples are treated with pH=7 chemical solution for 5 and 30 soaking days, respectively.

their emergence and geometry characteristics as shown in Fig. 14. The crack types can be categorized as wing crack, anti-wing crack, secondary crack, far-field crack and surface spalling. The wing crack initiates at the tips or a certain distance from the tips of the preexisting flaws, and usually propagates along the direction of the compressional stress to the end surface of the granite samples. The wing crack only displays the shape of the tensile crack trajectory and is always the first crack initiated from the rock sample containing single preexisting flaw (Wong and Einstein, 2009). The anti-wing crack has opposite propagation direction with the wing crack; therefore it is recognized as "anti-wing crack" by many researchers. The secondary crack initiates at the tips or a certain distance from the tips of the preexisting flaws. However, compared with the wing crack, the secondary crack usually initiates after the occurrence of wing crack and propagates along the direction of the compressional stress (tensile cracks) or the maximum principal stress (shear cracks) toward the end surface of the granite samples. The far-field crack usually does not initiate from the tips of the preexisting flaw. The far-field crack can develop into a tensile crack, but also can be a shear crack based on their propagation direction. The surface spalling mostly occurs at the surface of the tested granite specimens under large σ_3.

In gypsum and Carrara marble specimens with two parallel preexisting open flaws under compression test, the coalescence mode can be classified into 3 categories: non-coalescence, direct coalescence and indirect coalescence as shown in Fig. 15 (Wong and Einstein, 2009). The difference between the direct coalescence and the indirect coalescence is the location of crack coalescence. In direct coalescence, the crack coalescence point is closer to the reference line compared with the distance in indirect coalescence. Otherwise, the indirect coalescence refers to the mode in which the coalescence points are far away from the reference line, resulting from two or multiple cracks. The non-coalescence mode has no coalescence point between the two preexisting flaws.

5.1 Failure mode of intact granite specimens

Figure 16 shows the ultimate failure characteristics of the granite samples treated by pH = 2 chemical solutions for 30 days under different σ_3. For intact specimens treated by chemical solutions under different σ_3, one main shear

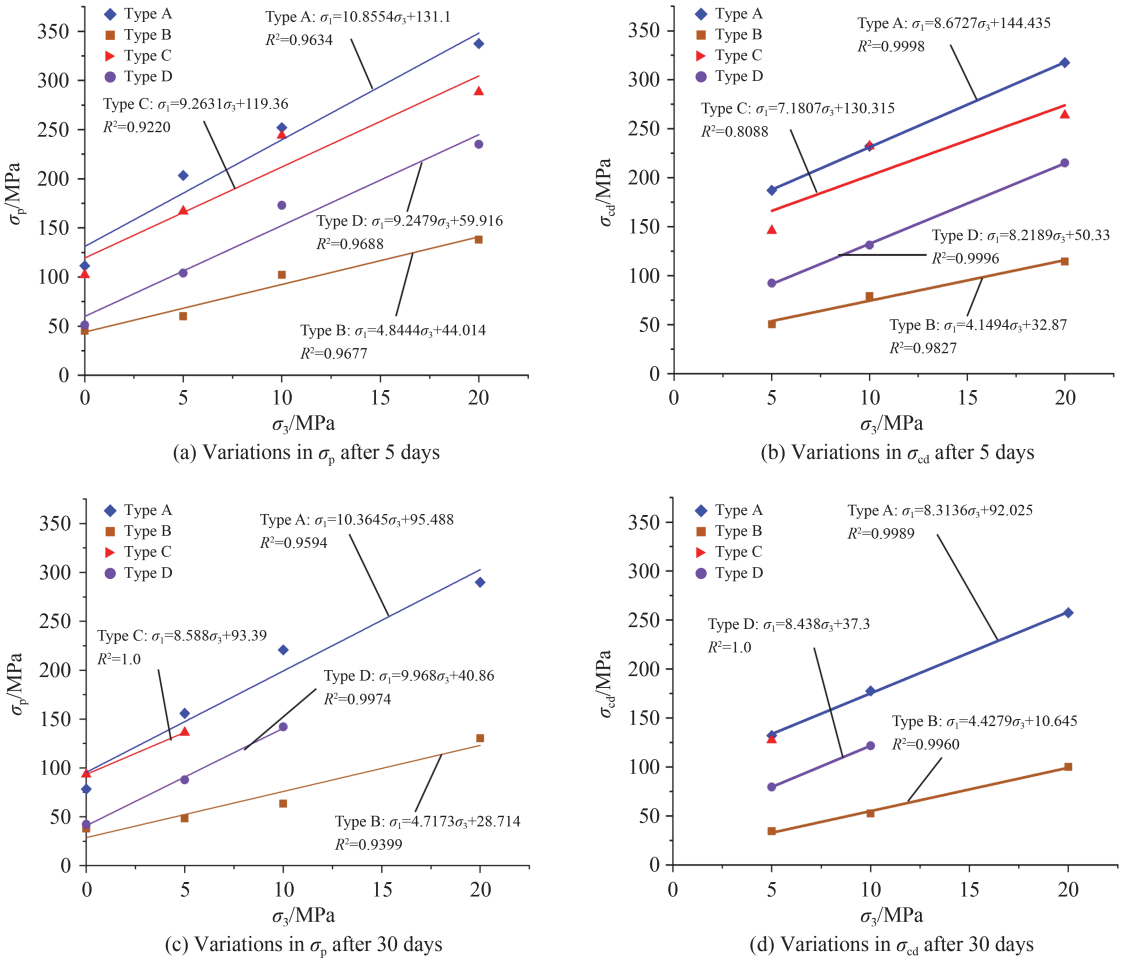

Fig. 12 Variations in peak axial stress σ_p and σ_{cd} versus confining pressure σ_3 varying from 0 to 20 MPa. The samples are treated with pH=12 chemical solution for 5 and 30 soaking days, respectively.

crack cutting through the specimen was generated. The angle (θ) between the main shear plane and compression load direction increases gradually with increasing the σ_3. Taking pH = 2 chemical solutions for 30 days as an exampling, θ increases from 21.76° to 26.69°, and to 34.79°, as the σ_3 increases from 5 MPa to 10 MPa and to 20 MPa. Because the pH value and soaking days have little influence on the ultimate failure of intact granite specimens, the results are not listed here.

5.2 Failure and crack coalescence mode of Type B pre-flawed granite specimens

The ultimate failure and crack coalescence of Type B pre-flawed granite specimens are shown in Fig. 17. Only one typical failure and crack coalescence mode is observed; therefore we only show three representative samples treated by pH = 2 chemical solution for 30 days under different σ_3 pressures. Due to the small inclination angle of α_1 and α_2, the failure mode of Type B samples always ends up with the connection of the secondary cracks initiated at the tips of the preexisting flaws. The secondary cracks propagate along the direction of the maximum principal stress until a macroscopic failure occurred. There was no wider crack on the surface of the tested specimens. With increasing the σ_3, the crack coalescence path becomes rougher. The effects of the pH value, soaking days and σ_3 on the ultimate failure mode and crack coalescence behavior of tested Type B specimens are not very significant, because the angles of the two flaws play a dominant role.

5.3 Failure and crack coalescence mode of Type C and D pre-flawed granite specimens

The ultimate failure states of surfaces of Type C specimens are shown in Fig. 18, and a sketch of surface cracks is also presented. Based on the cracking behaviors and propagation mechanisms, the main crack can be divided into five types, including wing crack, anti-wing crack, secondary crack, far-filed crack and surface spalling.

The ultimate failure mode and crack coalescence behavior contained at least two main crack types under triaxial compressions. When σ_3 = 5 MPa, there are no obvious shear plane on the surface of the specimens treated by different chemical solutions for 5 days.

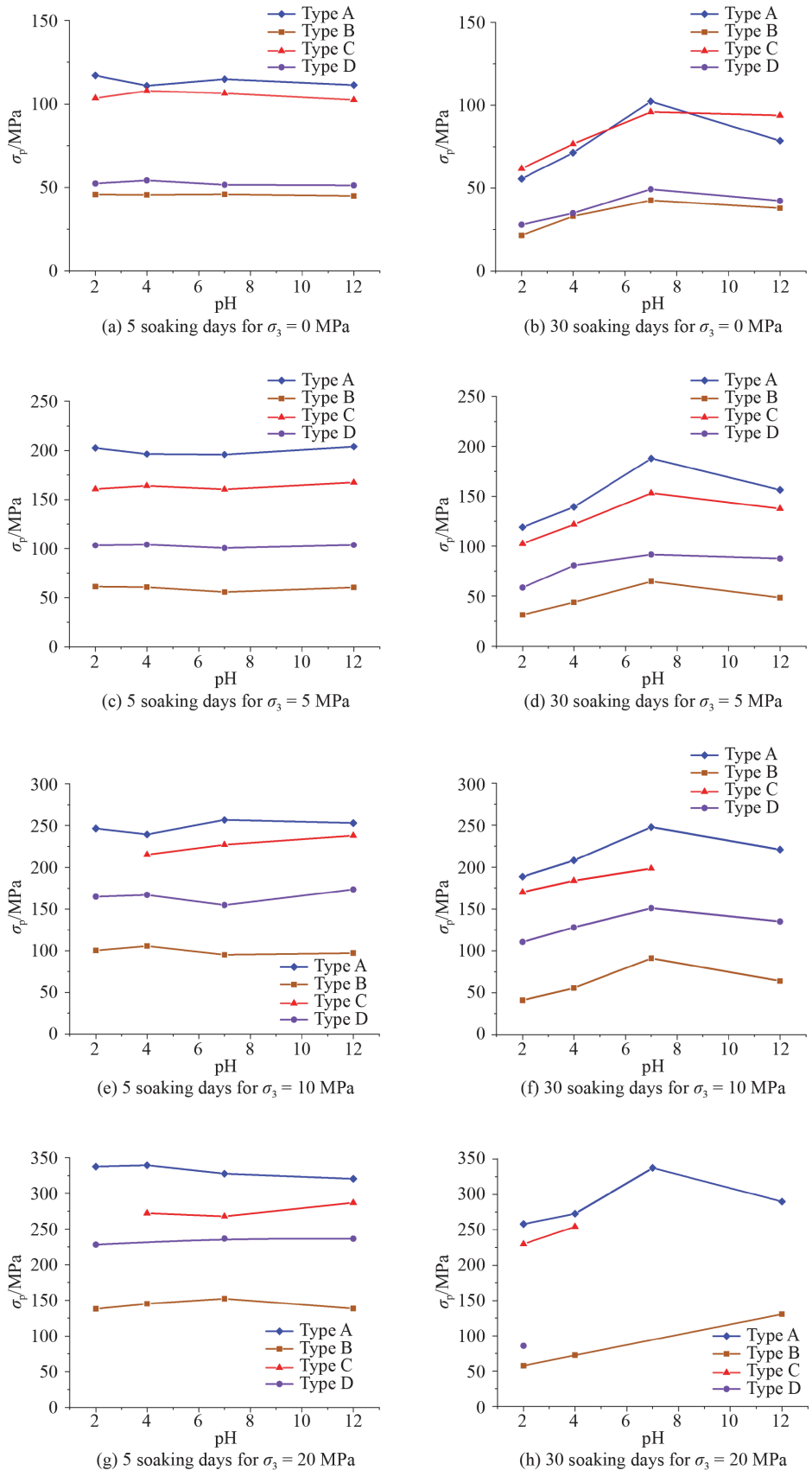

Fig. 13 Variations in peak axial stress σ_p versus pH for specimens under confining pressures of 0, 5, 10, 20 MPa and 5 and 30 soaking days, respectively.

Table 3 Peak strength and crack damage parameters of tested granite specimens in accordance with the linear Mohr-Coulomb criterion

Fracture mode	Soaking days	pH value	C_p/MPa	C_{cd}/MPa	φ_p/(°)	φ_{cd}/(°)
A	5	2	20.27	9.21	57.40	53.43
B	5	2	10.05	7.79	42.04	34.19
D	5	2	8.96	8.68	53.90	45.22
A	30	2	13.42	10.53	56.54	52.58
B	30	2	8.91	8.31	16.95	16.65
C	30	2	10.50	8.76	53.59	52.48
D	30	2	5.95	1.05	49.24	54.60
A	5	4	20.23	19.53	57.54	55.08
B	5	4	13.97	8.96	53.90	35.76
C	5	4	22.10	21.90	51.39	49.19
D	5	4	7.99	6.04	58.04	58.17
A	30	4	14.50	13.56	56.33	53.16
B	30	4	10.40	12.21	19.45	6.15
C	30	4	13.53	9.97	54.28	53.99
A	5	7	19.83	19.42	57.78	55.17
B	5	7	9.51	8.35	45.35	42.52
C	5	7	28.06	21.12	52.42	31.26
D	5	7	11.35	9.08	54.98	38.96
A	30	7	19.59	17.52	58.60	55.82
B	30	7	9.47	9.35	42.36	37.41
C	30	7	15.75	15.33	56.77	54.11
D	30	7	7.28	4.04	56.68	57.10
A	5	12	24.52	19.90	57.73	53.89
B	5	12	10.00	8.07	42.23	38.71
C	5	12	24.32	19.61	55.05	50.38
D	5	12	9.85	8.78	55.02	52.92
A	30	12	15.96	14.83	56.97	53.12
B	30	12	6.61	2.53	41.64	40.21
D	30	12	6.47	6.42	56.31	53.39

However, when the chemical corrosion day increased to 30 days, obvious shear plane can be found on the surface of these specimens except for C_4-30-b. With the increment of σ_3, a larger number of shear plane, drum shape and double-layered failure surface can be found accompanying with a loud sound when the tested specimens are failed. This indicates that σ_3 effectively restricts the lateral deformation of the specimens. Compared with specimens treated by chemical corrosion for 5 days, the crack coalescence only occurred at the specimens with 30 soaking days under a σ_3 of 20 MPa with indirect coalescence occurred at C_2-30-d and C_4-30-d, and direct coalescence occurred at C_7-30-d and C_{12}-30-d. The crack coalescence significantly occurs at specimens treated by chemical corrosion for 30 days under relatively large σ_3 (10 MPa and 20 MPa) except for C_{12}-5-c. It may be because that, under a longer chemical corrosion time, the chemical solution could sufficiently react with the minerals of the specimens, resulting in the changes in crack coalescence. Most of Type C specimens belong to the non-coalescence case because of the relatively large α_1 and α_2.

The ultimate failure surfaces and sketches of Type D specimens treated by chemical solutions with pH = 2–12 for 5 and 30 soaking days under σ_3 of 5–20 MPa are shown in Fig. 19. In the case of D_{12}-5-b, there was no crack initiated at the tips of left preexisting crack, which indicates that the wing crack, anti-wing crack and secondary crack do not necessarily initiate at the tips of all the preexisting flaws. Crack coalescence only occurred in D_2-30-c, D_4-5-c, D_4-30-b and D_7-30-d belonging to indirect coalescence. For the specimens under large σ_3,

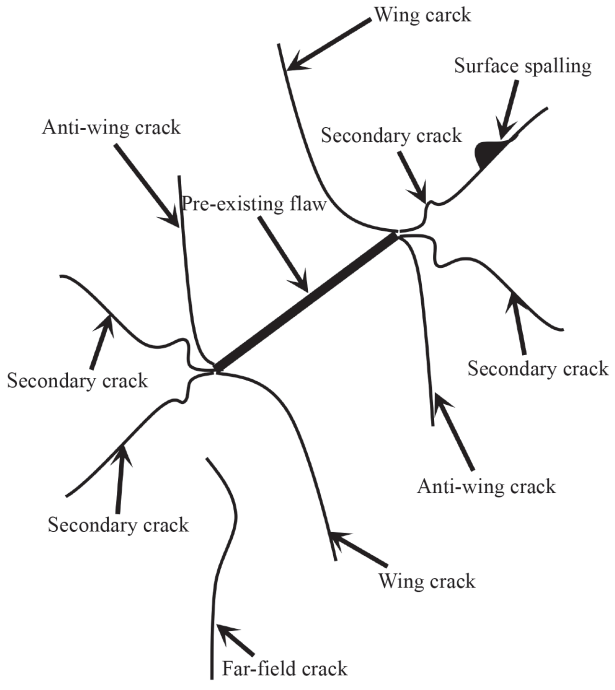

Fig. 14 Crack types observed in specimens with crack in compression (modified after Yang and Jing, 2011).

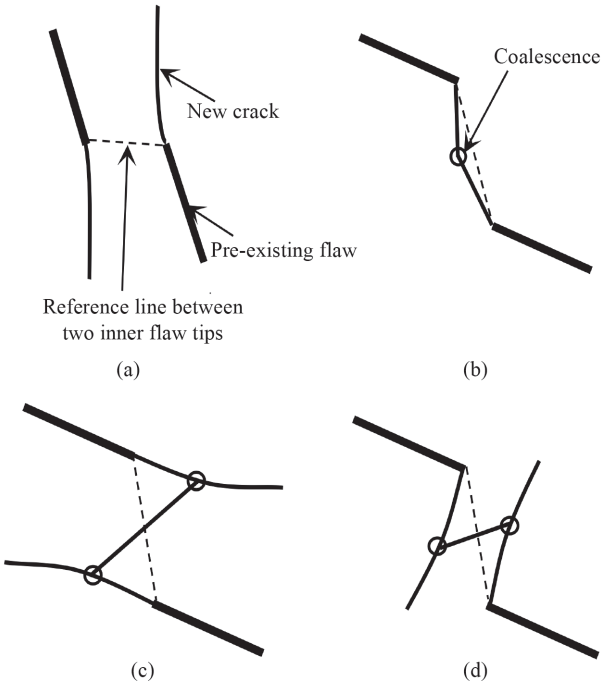

Fig. 15 Crack coalescence manners (modified slightly from Wong et al., 2008a; Yang et al., 2008): (a) non-coalescence, (b) direct coalescence, (c) and (d) indirect coalescence.

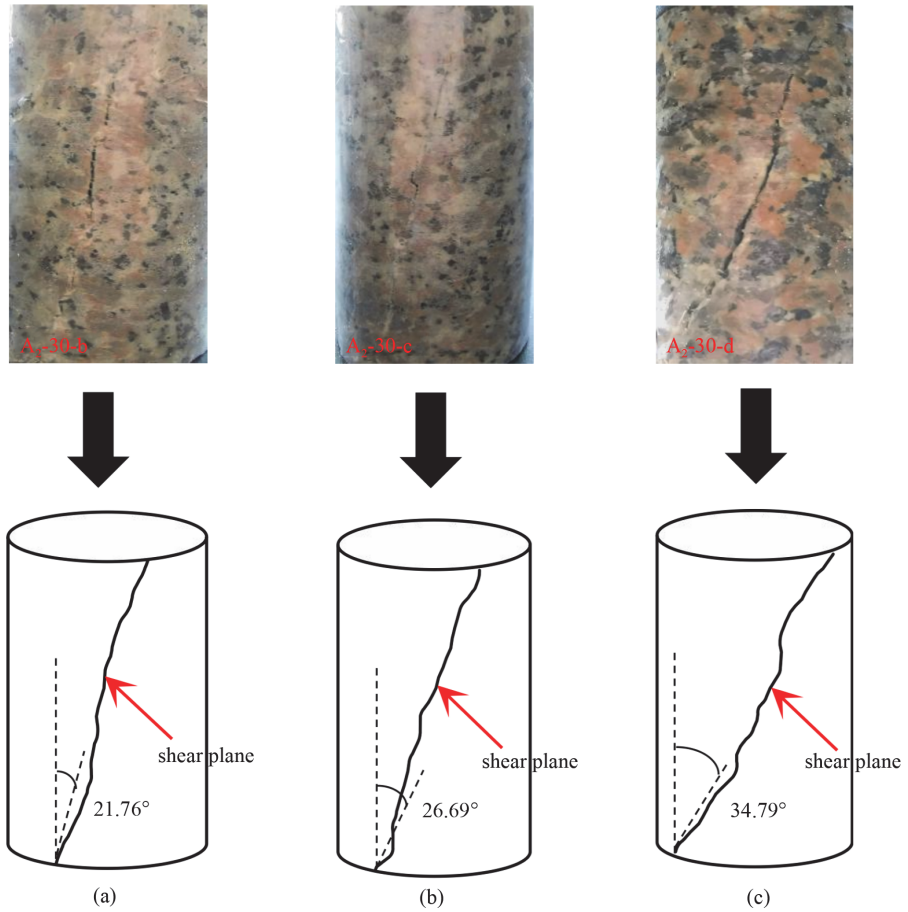

Fig. 16 Typical failure of the tested intact (type A) granite specimens treated with pH=2 chemical solution for 30 days under different confining pressures: (a) 5 MPa, (b) 10 MPa and (c) 20 MPa.

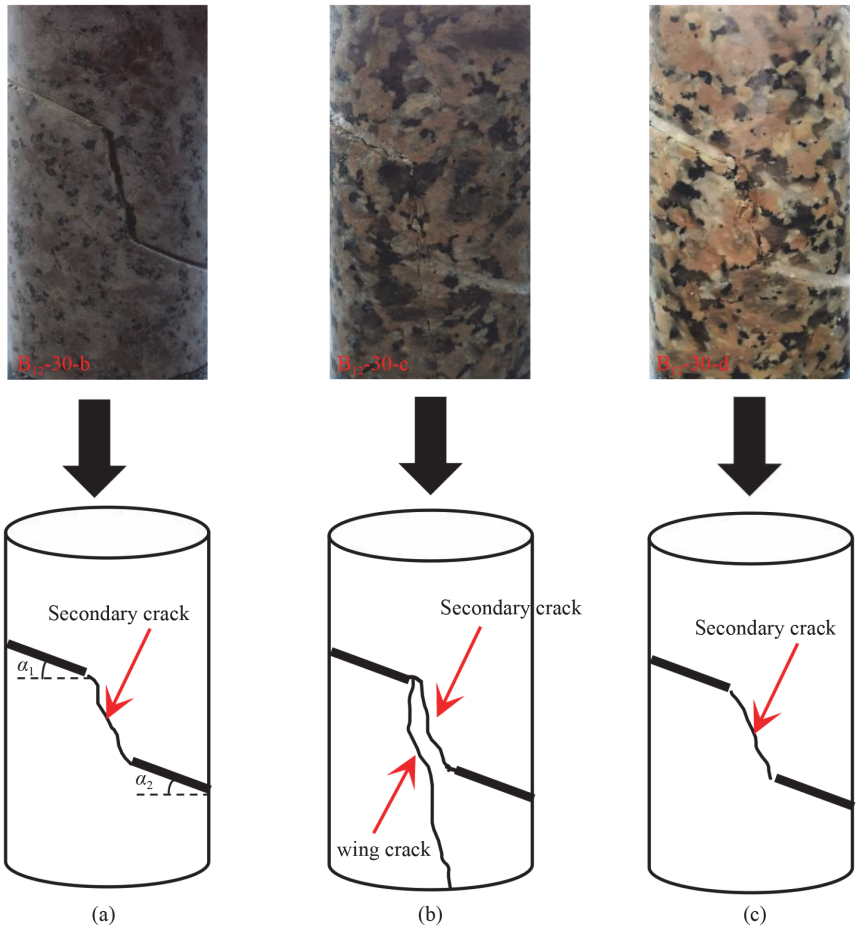

Fig. 17 Typical failure and crack coalescence of the tested type B granite specimens treated with pH = 2 chemical solution for 30 days under different confining pressures: (a) 5 MPa, (b) 10 MPa and (c) 20 MPa.

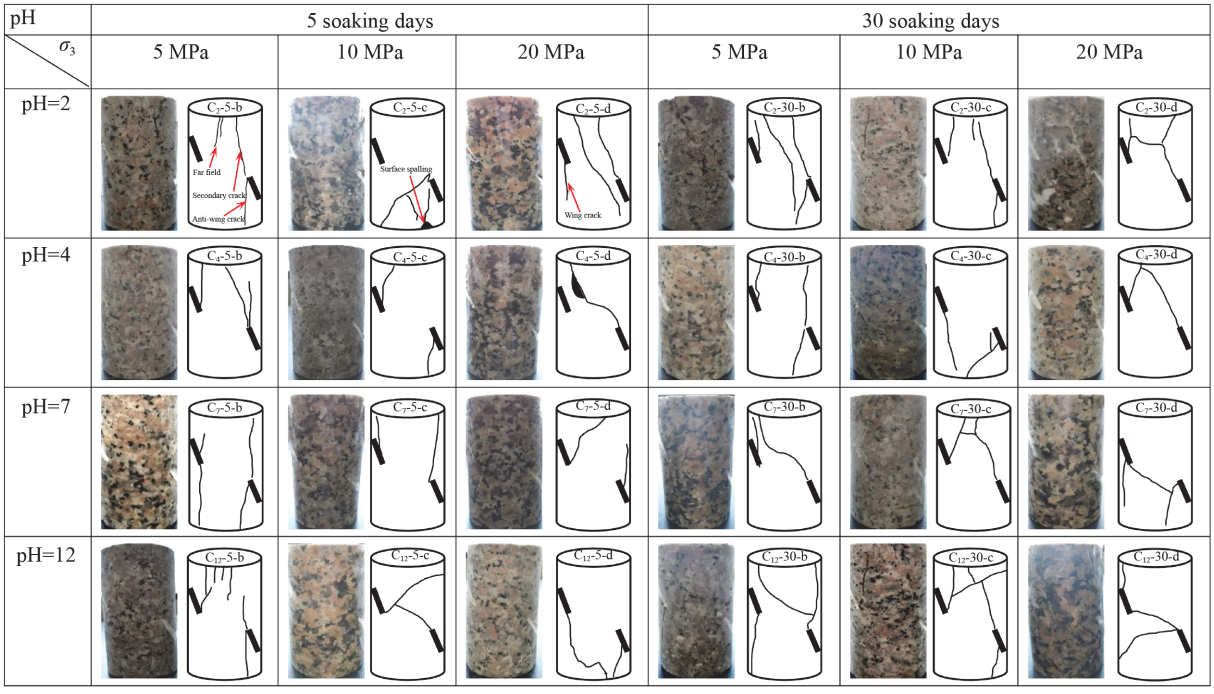

Fig. 18 Ultimate failure modes of Type C granite specimens treated with different chemical solutions for 5 and 30 days.

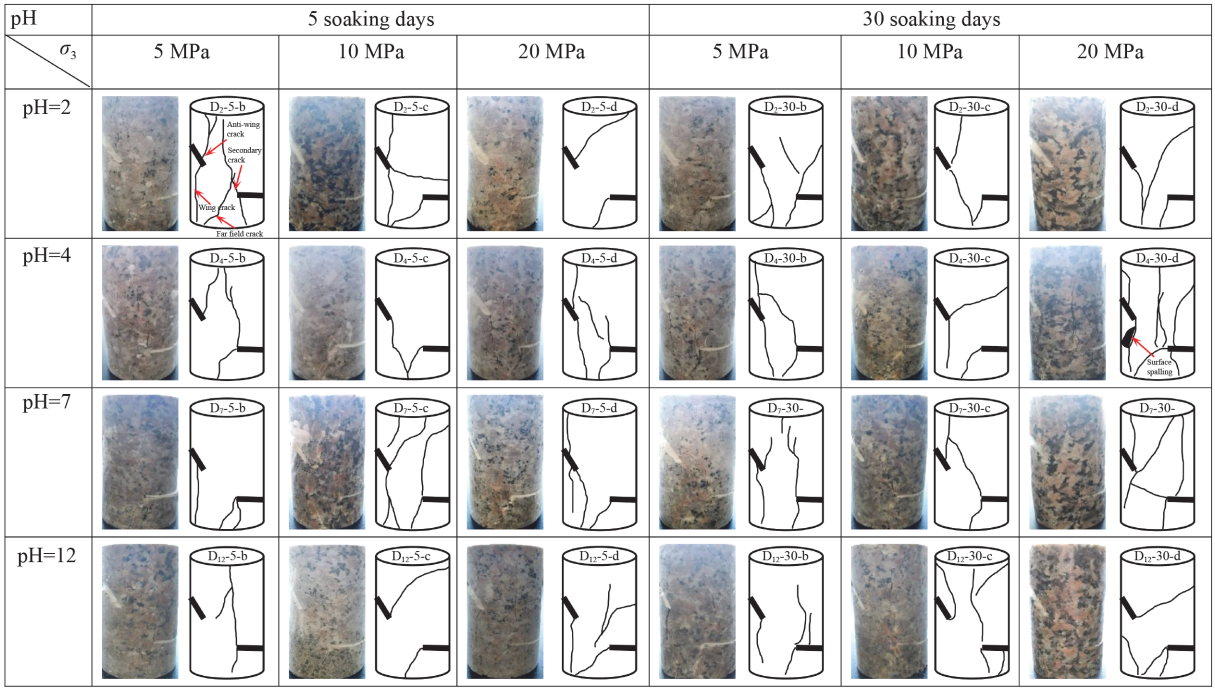

Fig. 19 Ultimate failure modes of Type D granite specimens treated with different chemical solutions for 5 and 30 days.

the propagated cracks are rough, resulting from the heterogeneity of granite materials. For the specimens treated by different chemical solutions for 5 or 30 days under different σ_3, the wing crack and anti-wing crack were also observed under the σ_3 of 20 MPa. However, the number of cracks is reduced compared with respect to the number of cracks generated in specimens at low σ_3 such as 5 MPa and 10 MPa. Therefore, the secondary cracks dominate the ultimate failure of tested specimens. The surface spalling only occurred in D_4-30-d under a σ_3 of 20 MPa, and the phenomenon of drum shape is easier to occur at a larger σ_3, which is similar to that in Type C. The ultimate failure mode and crack coalescence behavior of Types C and D specimens under triaxial compression test are affected by pH value of chemical solution, chemical corrosion time and σ_3, which is different from those of Types A and B specimens.

With the increasement of θ, the peak axial stresses of Type A samples have increased accordingly. However, the ultimate failure modes of Type B samples are the same with connections between two flaws. Therefore, the ultimate failure modes have no effect on the peak axial stresses of Type B samples. For Types C and D, the ultimate failure modes of these types are different with each other, which resulted in no obvious regular between the peak axial stress and ultimate failure modes. In the future, we should conduct numerical simulations on the development processes of cracks instead of the ultimate failure mode of granites to study the connections between the peak axial stress and the development of cracks.

6 Conclusions

The present study carried out triaxial compression tests on intact and pre-flawed granite specimens treated by chemical corrosion. The evolutions of stress-strain curves, critical stress for crack initiation, volume dilation, influence of the confining pressure σ_3 and pH value on peak strength were investigated. Finally, the ultimate failure and crack coalescence mode were analyzed and discussed.

The results show that the typical axial deviatoric stress-strain curves can be divided into four stages, including the stage of nonlinear deformation, the stage of the linear phase, the stage of the stress hardening and the stage of brittle failure. The granite specimens of four types subjected to different chemical solutions still show brittle failure when the σ_3 is smaller than 20 MPa. The peak axial deviatoric stresses of Type C with two preexisting relatively high-dip flaws has the least difference from those of Type A, followed by Type B with relatively low-dip flaws and Type D with both relatively low-dip and relatively high-dip flaws specimens. The Type B granite samples failed at a strain of approximately 0.4%–1.4%, which were smaller than those of Type D and Type C with 0.6%–2.5% and 0.7%–1.9%, respectively. Based on the Mohr-Coulomb criterion, the calculated values of the cohesion C and the internal friction angle φ are significantly depend on the arrangements of preexisting flaws, followed by the chemical corrosion time and pH value of the chemical solution. The H^+ ions of pH = 2 and pH = 4 and OH^- ions of pH = 12 chemical solutions

effectively reacted with the minerals of the tested samples, resulting in generation of new cracks. The cracks propagated and connected with other cracks or original flaws, eventually leading to a decrease in peak strength σ_p. The pH value and soaking days have little influence on the ultimate failure and crack coalescence mode of Types A and B specimens. The ultimate failure and crack coalescence mode of Type C and D specimens are robustly affected by pH value of chemical solution, corrosion time and σ_3.

Although 128 samples were used to investigate the mechanical behavior of granites treated after chemical corrosion, the specimens treated by real-time chemical corrosion were not taken into account in the present study, which will be investigated in our future works. Besides, the threshold of chemical corrosion time should be determined by setting more corrosion time. Finally, a numerical method that can simulate the coupled mechanical-chemical processes will be developed to characterize the failure process of granites under triaxial compression tests.

Acknowledgments This study has been partially funded by the National Key Research and Development Program of China, China (Grant No. 2020YFA0711800), the National Natural Science Foundation of China (Grant Nos. 51734009, 51979272, and 52179118), and Natural Science Foundation of Jiangsu Province, China (No. BK20211584). These supports are gratefully acknowledged.

References

Bombolakis E G (1968). Photoelastic study of initial stages of brittle fracture in compression. Tectonophysics, 6(6): 461–473

Ding W (2012). Study on the time-dependent characteristics of sandstone under chemical corrosion. App Mech Mater, 256–259: 174–178

Feng X T, Li S, Chen S (2004). Real-time computerized tomography (CT) experiments on sandstone damage evolution during triaxial compression with chemical corrosion. Int J Rock Mech Min Sci, 41(2): 181–192

Feng X T, Chen S, Li S (2001). Effects of water chemistry on microcracking and compressive strength of granite. Int J Rock Mech Min Sci, 38(4): 557–568

Han T, Shi J, Cao X (2016). Fracturing and damage to sandstone under coupling effects of chemical corrosion and freeze–thaw cycles. Rock Mech Rock Eng, 49(11): 4245–4255

Huang D, Gu D, Yang C, Huang R, Fu G (2016). Investigation on mechanical behaviors of sandstone with two preexisting flaws under triaxial compression. Rock Mech Rock Eng, 49(2): 375–399

Lee H, Jeon S (2011). An experimental and numerical study of fracture coalescence in pre-cracked specimens under uniaxial compression. Int J Solids Struct, 48(6): 979–999

Li H, Wong L N Y (2014). Numerical study on coalescence of pre-existing flaw pairs in rock-like material. Rock Mech Rock Eng, 47(6): 2087–2105

Li H, Yang D, Zhong Z, Sheng Y, Liu X (2018). Experimental investigation on the micro damage evolution of chemical corroded limestone subjected to cyclic loads. Int J Fatigue, 113: 23–32

Li N, Zhu Y, Su B, Gunter S (2003). A chemical damage model of sandstone in acid solution. Int J Rock Mech Min Sci, 40(2): 243–249

Lu S (2018). A global review of enhanced geothermal system (EGS). Renew Sustain Energy Rev, 81: 2902–2921

Luo J, Zhu Y, Guo Q, Tan L, Zhuang Y, Liu M, Zhang C, Zhu M, Xiang W (2018). Chemical stimulation on the hydraulic properties of artificially fractured granite for enhanced geothermal system. Energy, 142: 754–764

Sagong S, Bobet A (2002). Coalescence of multiple flaws in a rock-model material in uniaxial compression. Int J Rock Mech Min Sci, 39(2): 229–241

Maligno A R, Rajaratnam S, Leen S B, Williams E J (2010). A three-dimensional (3D) numerical study of fatigue crack growth using remeshing techniques. Eng Fract Mech, 77(1): 94–111

Miao S, Cai M, Guo Q, Wang P, Liang M (2016). Damage effects and mechanisms in granite treated with acidic chemical solutions. Int J Rock Mech Min Sci, 88: 77–86

Olasolo P, Juárez M C, Morales M P, D'Amico S, Liarte I A (2016). Enhanced geothermal systems (EGS): a review. Renew Sustain Energy Rev, 56: 133–144

Portier S, Vuataz F D, Nami P, Sanjuan B, Gérard A (2019). Chemical stimulation techniques for geothermal wells: experiments on the three-well EGS system at Soultz-sous-Forêts, France. Geothermics, 38(4): 349–359

Qiao L, Wang Z, Huang A (2017). Alteration of mesoscopic properties and mechanical behavior of sandstone due to hydro-physical and hydro-chemical effects. Rock Mech Rock Eng, 50(2): 255–267

Rathnaweera T D, Wu W, Ji Y, Gamage R P (2020). Understanding injection-induced seismicity in enhanced geothermal systems: from the coupled thermo-hydro-mechanical-chemical process to anthropogenic earthquake prediction. Earth Sci Rev, 205: 103182

Taron J, Elsworth D (2010). Coupled mechanical and chemical processes in engineered geothermal reservoirs with dynamic permeability. Int J Rock Mech Min Sci, 47(8): 1339–1348

Wong R H C, Chau K T (1998). Crack coalescence in a rock-like material containing two cracks. Int J Rock Mech Min Sci, 97(2): 147–164

Wong L N Y, Einstein H H (2008a). Crack coalescence in molded gypsum and carrara marble: part 1. Macroscopic observations and interpretation. Rock Mech Rock Eng, 42(3): 475–511

Wong L N Y, Einstein H H (2008b). Crack coalescence in molded gypsum and carrara marble: part 2. Microscopic observations and interpretation. Rock Mech Rock Eng, 42(3): 513–545

Wong L N Y, Einstein H H (2009). Systematic evaluation of cracking behavior in specimens containing single flaws under uniaxial compression. Int J Rock Mech Min Sci, 46(2): 239–249

Wong L N Y, Li H (2013). Numerical study on coalescence of two pre-existing coplanar flaws in rock. Int J Solids Struct, 50(22–23): 3685–3706

Xie S, Shao J, Xu W (2011). Influences of chemical degradation on mechanical behavior of a limestone. Int J Rock Mech Min Sci,

48(5): 741–747

Yang S, Jiang Y, Xu W, Chen X (2008). Experimental investigation on strength and failure behavior of pre-cracked marble under conventional triaxial compression. Int J Solids Struct, 45(17): 4796–4819

Yang S, Jing H (2011). Strength failure and crack coalescence behavior of brittle sandstone samples containing a single fissure under uniaxial compression. Int J Fract, 168(2): 227–250

Zhang X, Wong L N Y (2011). Cracking processes in rock-like material containing a single flaw under uniaxial compression: a numerical study based on parallel bonded-particle model approach. Rock Mech Rock Eng, 45: 711–737

Zhou H, Hu D, Zhang F, Shao J, Feng X (2016). Laboratory investigations of the hydro-mechanical–chemical coupling behaviour of sandstone in CO_2 storage in aquifers. Rock Mech Rock Eng, 49(2): 417–426